Morphogen Directed Coordination of GPCR Activity Promotes Primary Cilium Function for Downstream Signaling

Shariq S. Ansari[1], Miriam E. Dillard[1], Yan Zhang[1], Mary Ashley Austria[1,2], Naoko Boatwright[3], Elaine L. Shelton[3,4], Amanda Johnson[5], Brandon M. Young[6], Zoran Rankovic[6], Camenzind G. Robinson[5], John D. Schuetz[7], and Stacey K. Ogden[1]

[1]Department of Cell and Molecular Biology, [5]Cell and Tissue Imaging Center, [6]Department of Chemical Biology and Therapeutics, [7]Department of Pharmaceutical Sciences, St. Jude Children's Research Hospital, Memphis, TN 38105

[3]Department of Pediatrics, Monroe Carell Jr. Children's Hospital at Vanderbilt and Vanderbilt University Medical Center, [4]Department of Pharmacology, Vanderbilt University School of Medicine, Nashville, TN 37232

[2]Rhodes College Summer Plus Program, Memphis, TN 38112

Correspondence: Stacey.Ogden@stjude.org

Abstract

Primary cilium dysfunction triggers catastrophic failure of signal transduction pathways that organize through cilia, thus conferring significant pressure on such signals to ensure ciliary homeostasis. Intraflagellar transport (IFT) of cargo that maintains the primary cilium is powered by high ciliary cAMP. Paradoxically, Sonic Hedgehog (SHH) signaling, for which ciliary function is crucial, triggers a reduction in ciliary cAMP that could blunt downstream signaling by slowing IFT. We investigated this paradox and mapped a novel signal relay driven by SHH-stimulated prostaglandin E_2 that stabilizes ciliary cAMP flux through by activating $G\alpha_s$-coupled EP_4 receptor. Chemical or genetic blockade of the SHH-EP_4 relay cripples cAMP buffering, which leads to decreased intraciliary cAMP, short cilia, and attenuated SHH pathway induction. Accordingly, *$EP_4^{-/-}$* mice show pronounced ciliary defects and altered SHH-dependent neural tube patterning. Thus, SHH orchestrates a sophisticated ciliary GPCR-cAMP signaling network that ensures primary cilium fitness for a robust downstream signaling response.

Introduction

The Sonic Hedgehog (SHH) signaling pathway is a crucial regulator of morphogenesis and tissue homeostasis that when corrupted, leads to developmental disorders and cancers (Barakat et al., 2010). Cellular responses to Hedgehog family ligands are orchestrated through primary cilia, which are dynamic sensory organelles that grow and retract with the cell cycle and in response to extracellular cues. Each cell possesses a single primary cilium anchored to the basal body that allows for organization of myriad signal transduction cascades to control diverse cellular responses (Anvarian et al., 2019; Wheway et al., 2018). Despite the membrane of the primary cilium being contiguous with the plasma membrane, it maintains a distinct membrane lipid composition due to lipid metabolic enzymes that function at or near the ciliary base (Arensdorf et al., 2017; Findakly et al., 2021; Garcia et al., 2018; Mukhopadhyay and Rohatgi,

45 2014; Raleigh et al., 2018). In addition, a cytoplasmic diffusion barrier controls entry of soluble
46 proteins, allowing primary cilia to offer controlled environments for interpretation and
47 transduction of extracellular signals (Garcia et al., 2018; Shi et al., 2017; Ye et al., 2013).

48

49 The SHH pathway requires primary cilia for regulated activity in both the absence and presence
50 of ligand. The SHH receptor Patched (PTCH), signal transducer Smoothened (SMO), and GLI2
51 and GLI3 transcriptional effectors all function at or flux through the primary cilium depending
52 upon SHH activation status (Arensdorf et al., 2016; Petrov et al., 2017). In the absence of
53 ligand, SMO entry into primary cilia is restricted by PTCH-mediated reduction of activating
54 sterols in ciliary membranes (Kinnebrew et al., 2019; Kinnebrew et al., 2021; Kong et al., 2019) .
55 In this off state, the primary cilium facilitates phosphorylation of GLI2 and GLI3 proteins by cyclic
56 AMP-dependent protein kinase (PKA), which tags them for partial degradation that removes
57 their transcriptional activation domains (Aza-Blanc et al., 2000; Aza-Blanc et al., 1997; Bangs
58 and Anderson, 2017). SHH binding to PTCH attenuates PTCH-mediated sterol depletion,
59 leading to SMO ciliary enrichment, binding to sterol agonist(s), and signaling to block PKA-
60 promoted GLI truncation. This leads to accumulation of full-length GLI2/3 proteins that are
61 subsequently phosphorylated at activating PKA sites for nuclear translocation and target gene
62 induction (Niewiadomski et al., 2014; Umberger and Ogden, 2021). The molecular mechanisms
63 driving the SHH-stimulated ciliary switch between inhibitory and activating GLI phosphorylation
64 are not yet known.

65

66 Current models suggest dependency of SHH signaling on primary cilia evolved from the
67 specialized lipid composition of ciliary membrane, which allows control over availability of sterols
68 and oxysterols that activate SMO to instruct GLI activation (Kinnebrew et al., 2019; Kong et al.,

69 2019; Raleigh et al., 2018). Moreover, second messengers such as cAMP can be rapidly
70 modulated in primary cilia independently of second messengers in the cytoplasm due to minimal
71 cytoplasmic content and a functional diffusion barrier at the ciliary base (Hansen et al., 2020;
72 Truong et al., 2021). Consistent with this functionality, and the key role of PKA in controlling
73 ciliary GLI regulation, SHH signal output is highly sensitive to cAMP flux in the primary cilium
74 (Mukhopadhyay et al., 2013; Truong et al., 2021; Vuolo et al., 2015). Moreover, alteration of
75 primary cilium length, architecture, or protein trafficking capability that can skew ciliary cAMP
76 diffusion, trigger pronounced disruption of pathway regulation (He et al., 2014; Truong et al.,
77 2021). This places significant pressure on SHH to ensure ciliary fitness for efficient downstream
78 signaling, suggesting mechanisms that link active signaling with primary cilium homeostasis
79 may exist.

80

81 A general mechanism by which ciliary homeostasis is directly affected is through activation of
82 prostaglandin signaling by prostaglandin E_2 (PGE_2) activating the E-type prostanoid receptor 4
83 (EP_4). Studies in zebrafish support that PGE_2 to EP_4 signaling is crucial for ciliary elongation
84 because mutation of the PGE_2 transporter ABC Transporter C4 (ABCC4) results in reduced
85 numbers and lengths of both motile and primary cilia (Jin et al., 2014). EP_4 promotes ciliary
86 elongation by activating $G\alpha_s$ heterotrimeric G proteins to raise intracellular cAMP for
87 anterograde IFT (Besschetnova et al., 2010; Hansen et al., 2020). Thus, rapid shifts in primary
88 cilium cAMP concentration can lead to pronounced shortening or lengthening of the organelle
89 (Besschetnova et al., 2010; Hansen et al., 2020). Paradoxically, activation of SHH signaling can
90 lead to reduction in primary cilium cAMP concentration. This occurs through SHH-stimulated
91 exit of the constitutively active $G\alpha_s$-coupled G protein-coupled receptor (GPCR) GPR161 from
92 ciliary membrane. GPR161 exit is thought to lower ciliary cAMP to attenuate PKA-promoted
93 GLI2/3 truncation in some cell types (Mukhopadhyay et al., 2013). In addition, SMO is a GPCR

94 that can activate heterotrimeric G proteins of the $G\alpha_i$ family to lower cAMP (Barzi et al., 2011;
95 Ogden et al., 2008; Riobo and Manning, 2007), raising the possibility that induction of SHH
96 signaling could hinder its own activity by reducing ciliary length. The fail-safes that prevent this
97 from occurring are not known.

98

99 We previously reported that SHH activates cytosolic phospholipase A2α ($cPLA_2$) to produce the
100 PGE_2 precursor arachidonic acid (Arensdorf et al., 2017). This occurs through SMO-mediated
101 activation of $G\alpha_i\beta\gamma$ heterotrimeric G proteins, which induce $cPLA_2$ through direct βγ binding.
102 Inhibition of $cPLA_2$ attenuates agonist-induced SMO ciliary translocation and blunts the GLI
103 response, supporting a role for arachidonic acid or one of its metabolites in amplification of the
104 SHH signal. Consistent with this notion, arachidonic acid directly targets the transmembrane
105 domain of active SMO to promote its ciliary entry (Arensdorf et al., 2017). Roles for arachidonic
106 acid metabolites in promoting SHH signaling output have not yet been defined.

107

108 Herein, we report that SHH-stimulated activation of $cPLA_2$ links SHH signal induction with ciliary
109 length control through production of PGE_2. We find that SHH stimulates production and export
110 of PGE_2 through cyclooxygenase (COX) and ABCC4, respectively, to activate ciliary $G\alpha_s$-
111 coupled EP_4. This provides a mechanism by which SHH buffers cAMP flux to stabilize primary
112 cilium length. Genetic elimination or small molecule inhibition of SHH-to-EP_4 signaling corrupts
113 primary cilium cAMP control, shortens primary cilia, alters SMO ciliary entry, and reduces SMO
114 signaling to GLI2/3. Accordingly, mice lacking EP_4 function have defective primary cilia and
115 show neural tube patterning defects indicative of compromised SHH signaling. As such, we
116 propose the SHH pathway evolved to link with prostaglandin signaling to tightly control primary

117 cilium cAMP for optimal function of the organelle from which it initiates its downstream signaling
118 responses.

119

120 **Results**

121 *ABCC4 loss shortens primary cilia and reduces SHH signaling output.*

122 Genetic studies in zebrafish revealed that the ABCC4 transporter is crucial for ciliogenesis *in*
123 *vivo*, and further, ABCC4 knockdown reduces ciliary lengths in cultured mammalian cells (Jin et
124 al., 2014). Given the pronounced sensitivity of canonical SHH signaling to alteration of ciliary
125 length (Caspary et al., 2007; He et al., 2014; Larkins et al., 2011), we sought to determine
126 whether loss of ABCC4 would lead to ciliary defects that alter SHH pathway activity. To quantify
127 the impact of ABCC4 loss on ciliary length in NIH-3T3 cells, we compared primary cilia of wild
128 type and CRISPR/Cas9-generated *ABCC4*$^{-/-}$ NIH-3T3 cells in the presence and absence of
129 control conditioned media or conditioned media containing the amino-terminal SHH signaling
130 domain, SHH-N (hereafter referred to as SHH, Figure 1A). Ciliary lengths of control and
131 *ABCC4*$^{-/-}$ cells were determined by analyzing acetylated α–tubulin marked cilia using confocal
132 imaging and LAS X software. Primary cilia of *ABCC4*$^{-/-}$ cells were on average ~25% shorter than
133 cilia of control NIH-3T3 cells in both control and SHH-treated cells (Fig. 1A-B).

134

135 To determine whether ciliary length reduction in *ABCC4*$^{-/-}$ cells would impact SHH pathway
136 activity, we tested for alteration of ligand-induced ciliary accumulation of the SHH signal
137 transducing protein SMO in *ABCC4*$^{-/-}$ cells. Localization of endogenous SMO to the primary
138 cilium was measured by quantifying immunofluorescence signal intensity of ciliary SMO protein
139 using confocal microscopy. Despite *ABCC4*$^{-/-}$ cells having shorter primary cilia than control cells,

140 SHH-induced SMO ciliary enrichment was comparable between the two cell populations (Figure
141 1C). Whereas modest SMO signal intensities were recorded in primary cilia of control
142 conditioned media-treated cells, significant ciliary enrichment of SMO occurred in cells treated
143 with SHH-CM, indicating that SMO ciliary translocation is not directly regulated through ABCC4
144 effects on primary cilium length (Fig. 1C). Despite the observed ciliary enrichment of SMO in
145 *ABCC4*$^{-/-}$ cells, its ability to activate GLI transcriptional effectors was nonetheless compromised.
146 SHH target genes *Ptch1* and *Gli1* were induced to significantly lower levels in *ABCC4*$^{-/-}$ cells
147 compared to control cells (Fig. 1D), indicating that ciliary length alteration resulting from ABCC4
148 loss can directly impact SHH pathway activity.

149

150 ABCC4 is reported to influence ciliogenesis by exporting PGE_2, which activates EP_4 receptors
151 on ciliary membranes to drive anterograde IFT for ciliary elongation and cargo trafficking (Figure
152 1E) (Besschetnova et al., 2010; Jin et al., 2014). To determine whether decreased PGE_2
153 secretion was responsible for reduced primary cilia lengths of *ABCC4*$^{-/-}$ cells, ELISAs were
154 performed to calculate PGE_2 levels in conditioned media collected from control and knockout
155 cells (Fig. 1F). Basal PGE_2 secretion was similar between control and *ABCC4*$^{-/-}$ cells,
156 suggesting alternative export mechanisms likely allow for basal PGE_2 release in the absence of
157 ABCC4 function. Consistent with our previous report that SHH stimulation results in production
158 of the PGE_2 precursor arachidonic acid (Arensdorf et al., 2017), control cells significantly
159 increased PGE_2 export following SHH exposure (Figure 1E-F). This increase was blocked by
160 pretreatment with the inverse SMO agonist cyclopamine and by inhibition of COX2, which
161 generates PGE_2 from arachidonic acid (Coxib, Figure 1F). As such, the PGE_2 exported from
162 SHH-stimulated cells is likely generated through SHH-induced arachidonic acid production.
163 Notably, *ABCC4*$^{-/-}$ cells did not increase PGE_2 secretion in response to SHH pathway activation
164 (Figure 1F), suggesting ABCC4 is crucial for SHH-stimulated release of prostaglandin.

165

166 *$cPLA_2$ contributes to ciliary length control downstream of SHH.*

167 To determine whether $cPLA_2$ activation downstream of SMO provides arachidonic acid
168 substrate for PGE_2 production and export, we tested the effects of $cPLA_2$ inhibition on PGE_2
169 release and primary cilium length using murine kidney inner medullary collecting duct (IMCD3)
170 cells. IMCD3 cells provide a robust model for investigation of primary cilium biology because
171 they are SHH responsive and produce longer primary cilia than NIH-3T3 cells (Besschetnova et
172 al., 2010; Jiang et al., 2019). We first tested whether, like NIH-3T3 cells, IMCD3 cells secreted
173 PGE_2 in response to SHH pathway activation. Indeed, ELISA of conditioned media from SHH-
174 stimulated IMCD3 cells showed accumulation of PGE_2 that was blocked by cyclopamine pre-
175 treatment (Figure 2A). SHH-stimulated PGE_2 secretion was also blocked by pre-treatment with
176 the specific $cPLA_2$ inhibitor giripladib (GIRI) (Duvernay et al., 2015; Thotala et al., 2013),
177 supporting that the SHH-stimulated pool of arachidonic acid generated by $cPLA_2$ provides a
178 source for PGE_2 production (Figure 2A).

179

180 To determine whether inhibition of $cPLA_2$ would reduce ciliary lengths in IMCD3 cells, we
181 treated cells with GIRI or vehicle control in the absence and presence of SHH, and measured
182 lengths of acetylated α-tubulin-marked primary cilia. Primary cilia of IMCD3 cells showed an
183 average length of approximately ~5 μm in control and SHH-stimulated conditions and were
184 shortened by approximately 40% to an average of ~3 μm at the highest GIRI concentration
185 tested (Figure 2B-C). Consistent with the ability of the $cPLA_2$ product arachidonic acid to
186 promote SMO ciliary entry (Arensdorf et al., 2017), we observed reduced SHH-stimulated SMO
187 accumulation in primary cilia following GIRI treatment. Despite this, SHH-stimulated GPR161

188 ciliary exit occurred normally, indicating its ciliary trafficking is unaltered by $cPLA_2$ inhibition
189 (Supplementary Figure 1A).

190

191 To test whether similar changes in ciliary lengths would occur following direct inhibition of PGE_2
192 production, we quantified ciliary length changes following COX2 inhibition. Coxib treatment
193 reduced ciliary lengths similarly to GIRI treatment, indicating that arachidonic acid metabolism
194 provides PGE_2 for ciliary length control in IMCD3 cells (Figure 2C'). Importantly, ciliary lengths
195 of GIRI-treated cells could be rescued by addition of supplemental arachidonic acid or PGE_2 to
196 cell culture medium (Supplementary Figure 1), indicating ciliary length alteration was a specific
197 effect of PGE_2 depletion. Moreover, supplemental arachidonic acid increased average primary
198 cilium length in SHH-stimulated cells (Supplementary Figure 1B-C), further supporting a positive
199 role for arachidonic acid in ciliary length control downstream of SHH. Curiously, whereas
200 supplemental PGE_2 efficiently rescued GIRI-induced ciliary shortening in the absence of SHH
201 stimulation, it did not rescue short cilia in its presence (Supplementary Figure 1D-E). We do not
202 know why supplemental arachidonic acid could rescue ciliary lengths in SHH-stimulated cells
203 while PGE_2 could not. However, we speculate that arachidonic acid metabolites in addition to
204 PGE_2 may contribute to ciliary fitness downstream of SHH. Consistent with this possibility,
205 arachidonic acid derived leukotrienes are reported to contribute to SHH-regulated neurite
206 projection (Bijlsma et al., 2008).

207

208 We next tested whether $cPLA_2$ inhibition would impact primary cilia lengths in human cells by
209 treating SHH-stimulated retinal pigmented epithelial (RPE1) cells with GIRI and quantifying
210 length changes as above. Primary cilia of RPE1 cells treated with GIRI prior to SHH-CM

211 treatment were approximately 25% shorter than cells treated with vehicle (Figure 2D). As such,
212 the link between SHH activation of $cPLA_2$ and ciliary length control is conserved.

213

214 Given the established connection between PGE_2 signaling and anterograde ciliary IFT (Jin et
215 al., 2015; Jin et al., 2014), we hypothesized $cPLA_2$ might serve as a general modulator of ciliary
216 fitness through its ability to produce the PGE_2 precursor arachidonic acid. Alternatively, $cPLA_2$
217 linkage to primary cilium function could occur specifically in the context of SHH signaling due to
218 its activation downstream of SMO (Arensdorf et al., 2017). To distinguish between these
219 possibilities, we tested for SHH-induced changes in expression of genes linked to primary cilium
220 function in control and GIRI-treated IMCD3 cells (Supplementary Figure 2). Whereas SHH did
221 not induce pronounced changes across the ciliary gene panel, GIRI treatment led to greater
222 than 2.5-fold expression changes in 13 of the 84 genes probed (Supplementary Figure 2A-B).
223 Strikingly, the effect of $cPLA_2$ inhibition on ciliary gene expression was amplified by SHH-
224 treatment. In SHH-stimulated cells, 32 genes showed pronounced expression changes
225 indicative of altered ciliary function upon combining $cPLA_2$ inhibition with SHH pathway
226 activation (Supplementary Figure 2C). Thus, $cPLA_2$ contributions to ciliary fitness are likely
227 linked to its function in the SHH signal relay.

228

229 *EP_4 activation provides ciliary length control for SHH signaling to GLI.*

230 PGE_2 promotes ciliogenesis by activating the prostaglandin EP_4 receptor, which signals through
231 $G\alpha_s$ heterotrimeric G proteins to raise ciliary cAMP for anterograde IFT (Besschetnova et al.,
232 2010; Jin et al., 2014). To determine whether PGE_2 produced downstream of SHH signals
233 through EP_4 to maintain ciliary length, primary cilia lengths were measured in control and SHH-
234 stimulated IMCD3 cells exposed to the EP_4 inhibitor L161,982 (Cherukuri et al., 2007). Primary

235 cilia of SHH-stimulated IMCD3 cells treated with increasing concentrations of L161,982
236 shortened in a dose-dependent manner, supporting a role for EP_4 in promoting ciliary length
237 homeostasis in SHH-stimulated cells (Figure. 3A). Like what occurred upon $cPLA_2$ inhibition,
238 short cilia resulting from EP_4 inhibition showed reduced accumulation of endogenous SMO
239 following SHH stimulation (Figure 3B-C). This led to compromised activation of GLI
240 transcriptional effectors downstream of SHH, as indicated by reduced expression of *Gli1* and
241 *Ptch1* target genes in both NIH-3T3 and IMCD3 cells (Figure 3D-D'). Importantly, mouse
242 embryonic fibroblasts (MEFs) generated from $EP_4^{-/-}$ embryos had shorter primary cilia than
243 control MEFs in both basal and SHH-stimulated conditions, supporting L161,982 effects were
244 the result of on-target EP_4 inhibition (Figure 3E-F). SHH-stimulated SMO ciliary enrichment was
245 also attenuated in EP_4 knockout MEFs (Figure 3E,G), indicating that altered primary cilium
246 fitness resulting from compromised PGE_2/EP_4 signaling adversely affects SHH signal
247 transduction.

248

249 *EP_4 signaling buffers ciliary cAMP flux following SHH pathway activation.*

250 Given that the principal influence of EP_4 on ciliary length occurs through its activation of $G\alpha_S$-
251 coupled heterotrimeric G proteins, we hypothesized the ciliary architecture and SHH signaling
252 defects observed following EP_4 inhibition were the result of disrupted ciliary cAMP flux (Figure
253 4A). To test this, we used a primary cilium-localized fluorescent sensor system to track ciliary
254 cAMP flux in control and SHH-stimulated IMCD3 cells in which EP_4 activity was disrupted
255 (Figure 4B-C and Supplementary Figure 3). We first determined whether pretreatment with
256 $cPLA_2$ or EP_4 inhibitors would compromise the ability of the adenylyl cyclase activator forskolin
257 (FSK) to raise cAMP in primary cilia. FSK stimulation of control cells showed a rapid and robust
258 increase in ciliary cAMP concentration, demonstrating efficacy of the cAMP sensor for

259 measuring ciliary cAMP flux in IMCD3 cells (Figure 4B-B', red, Supplementary Figure 3A-B).
260 Consistent with the reduced ciliary lengths and altered ciliary function that occurred following
261 $cPLA_2$ and EP_4 inhibition (Figures 2-3), pretreatment of IMCD3 cells with either GIRI or
262 L161,982 prior to FSK stimulation blunted ciliary cAMP accumulation by approximately ~30%
263 (Figure 4B-B', red vs. blue). Thus, attenuation of PGE_2 production or inhibition of its receptor
264 EP_4 disrupts ciliary cAMP flux.

265

266 To test the impact of attenuated EP_4 signaling on SHH-induced changes in ciliary cAMP, we
267 treated cells with the direct SMO agonist SAG in the absence or presence of EP_4 inhibitor
268 L161,982 (Figure 4C). Likely due to the ability of activated SMO to both couple with $G\alpha_i$ and to
269 induce exit of $G\alpha_s$-coupled GPR161 from primary cilia, the FSK response was both delayed and
270 blunted by SAG treatment (Figure 4C, red vs blue). Despite these reductions, primary cilia of
271 both control and SAG-treated cells equilibrated to similarly elevated cAMP concentrations. This
272 equilibration of ciliary cAMP following SAG treatment was blocked by EP_4 inhibition (Figure 4C,
273 green vs. blue). Thus, the SHH-$cPLA_2$-EP_4 signaling axis is likely induced to buffer against
274 sustained ciliary cAMP reduction following SHH pathway activation.

275

276 If cAMP generated through SHH-to-EP_4 signaling promotes IFT for ciliary length maintenance
277 and optimal SHH responsiveness, we reasoned that directly raising ciliary cAMP following EP_4
278 inhibition should restore ciliary length and rescue SHH pathway activity. To affect ciliary cAMP
279 in a controlled manner, we used a validated optogenetic system (Truong et al., 2021). In this
280 system, bacterial photoactivatable adenylyl cyclase (bPAC) is targeted to primary cilia and
281 activated to specifically raise ciliary cAMP by exposure to blue light (Supplementary Figure 4A).
282 IMCD3 cells were engineered to stably express ciliary bPAC, and then analyzed for ciliary

283 length changes following blue light stimulation (Figure 4D-F and Supplementary Figure 4). To
284 establish whether effects of blue light exposure were specific to bPAC-induced cAMP
285 modulation, we first confirmed that ciliary length did not change in wild type IMCD3 cells upon
286 blue light exposure. Although primary cilia of wild type cells were generally longer than those of
287 bPAC-expressing cells, they were not affected by blue light (Figure 4D and Supplementary
288 Figure 4B-C). Consistent with the established ability of cAMP to promote ciliary elongation,
289 IMCD3-bPAC cells exposed to blue light increased average primary cilium length by
290 approximately 25%, restoring the reduced average baseline length back to what is observed in
291 control cells (Figure 4D and Supplementary Figure 4B-C). These results support the feasibility
292 of using the ciliary bPAC system to directly manipulate ciliary length. Armed with this tool, we
293 next tested whether short cilia of EP_4-inhibited cells could be lengthened by stimulating bPAC
294 activity. Consistent with the hypothesis that reduced primary cilium length following EP_4
295 inhibition resulted from a failure in cAMP flux control, we observed that blue light partially
296 restored ciliary length in SHH-stimulated, L161,982-treated cells (Figure 4E and Supplementary
297 Figure 4D-F). Blue light increased average ciliary lengths by 25% following L161,982 treatment
298 in both the absence and presence of SHH, raising the possibility that SHH signal induction could
299 be partially restored by EP_4 cAMP bypass. To test this, we quantified SMO ciliary enrichment in
300 bPAC-expressing cells exposed to L161,982 in the absence of blue light or after 180 minutes of
301 blue light exposure. Consistent with the ability of blue light-induced cAMP to partially reverse
302 ciliary length reduction resulting from EP_4 inhibition, SHH-stimulated SMO ciliary enrichment
303 was also partially restored in blue light exposed cells (Figure 4F, column 3 vs.4). Intriguingly,
304 SHH-stimulated enrichment of SMO in vehicle treated cells was enhanced by blue light
305 stimulation, suggesting that augmenting cAMP production in cells with an active SHH pathway
306 may enhance anterograde IFT to facilitate increased SMO ciliary loading (Figure 4F, column 2
307 vs. 5). Thus, tight modulation of ciliary cAMP is likely crucial for appropriate SMO ciliary
308 trafficking behavior.

309

310 *EP_4 is required for ciliary fitness and SHH signaling during neural tube development.*

311 Having established a cell-biological connection between SHH signaling and EP_4-regulated
312 primary cilium length homeostasis, we next sought to determine whether compromised EP_4
313 activity would affect primary cilium fitness to impact SHH signaling *in vivo*. To do so, we
314 analyzed developing neural tubes of *EP4*$^{-/-}$ mice for ciliary morphology and ventral neural fate
315 specification (Segi et al., 1998). During neural tube development, SHH signals in a graded
316 manner from the notochord and ventral floor plate to instruct ventral cell fates. Ventrally-
317 localized cells nearest the floor plate are exposed to high concentrations of SHH, and thus
318 activate highest threshold transcriptional targets that enforce ventral fates. More dorsally-
319 localized cells are exposed to little or no SHH, and thus activate dorsally-restricted
320 transcriptional programs (Ericson et al., 1997; Patten and Placzek, 2000; Ribes and Briscoe,
321 2009). To determine whether ciliary fitness of the neuroepithelium was altered by EP_4 loss *in*
322 *vivo*, we examined primary cilium morphology along the luminal surface of neural tubes from
323 E9.5 $EP_4^{+/-}$ and $EP_4^{-/-}$ mice using scanning electron microscopy (Figure 5A). Primary cilia on
324 apical membranes of cells lining neural tube lumen in $EP_4^{-/-}$ embryos were significantly shorter
325 than cilia of heterozygous littermate control embryos (Figure 5A-B). Whereas primary cilia of
326 ventral cells in control neural tubes averaged ~0.9 μm, ventral cilia in knockout embryos showed
327 an approximate 30% length reduction to an average length of ~0.6μm. Similar primary cilium
328 length differences between control and knockout embryos were observed in dorsal neural tube
329 scans, indicating that EP_4 is crucial for primary cilium length maintenance in the developing
330 neural tube. Curiously, primary cilia of more dorsally localized cells from control neural tubes
331 showed modestly reduced lengths compared to ventral cell cilia. Although ciliary length
332 differences between cilia of ventrally and dorsally localized luminal cells failed to reach
333 significance, we speculate the trend could indicate that sustained high-threshold SHH

334 stimulation that occurs in ventral cells may positively impact ciliary length by promoting EP_4
335 activity. Consistent with this hypothesis, the modest ventral/dorsal ciliary length difference was
336 not evident in *EP4*$^{-/-}$ neural tube sections (Figure 5B).

337

338 To test whether neural tube ciliary length alteration resulting from EP_4 loss compromised SHH-
339 dependent neural tube progenitor domain specification, we examined expression of the ventral
340 fate marker *Olig2* and intermediate marker *Pax6*, which is inhibited by high SHH signaling
341 (Ericson et al., 1997; Ribes and Briscoe, 2009). Because specification of ventral progenitor
342 domains is highly sensitive to signal attenuation, monitoring their induction allows for reliable
343 reporting of SHH pathway activity (Ribes and Briscoe, 2009). Comparison of knockout and
344 heterozygous littermate control neural tubes revealed consistent reduction of the SHH-
345 dependent *Olig2*-positive progenitor population in *EP*$_4^{-/-}$ animals (n=4). Conversely, the
346 expression domain of the intermediate fate marker *Pax6* was not significantly altered (Figure
347 5C). Thus, ciliary dysfunction resulting from EP_4 loss compromises SHH-directed ventral fate
348 specification *in vivo*.

349

350 **Discussion**

351 The study presented here identifies a previously unrecognized SHH-to-EP_4 signal relay that
352 stabilizes ciliary cAMP flux for primary cilium length homeostasis. In this relay, SHH counteracts
353 ciliary cAMP reduction that occurs following SMO activation and GPR161 ciliary exit by
354 activating $cPLA_2$ for production of PGE_2 and activation of $G\alpha_s$-coupled-EP_4. This increases
355 ciliary cAMP to power anterograde trafficking for maintenance of primary cilium length.
356 Disruption of prostaglandin signaling compromises ciliary cAMP control downstream of SHH,
357 leading to altered ciliary morphology, attenuated SMO ciliary accumulation, reduced GLI-

358 mediated target gene activation, and disruption of ventral neural tube patterning. Thus, we
359 propose SHH evolved to link with PGE_2/EP_4 signaling, via $cPLA_2$, activation for primary cilium
360 length control due to its strict dependency on the organelle for regulation of its downstream
361 effectors (Arensdorf et al., 2017; Arensdorf et al., 2016; Mukhopadhyay and Rohatgi, 2014).
362 Importantly, all experiments in this study were performed using cells with endogenously
363 expressed and genetically or chemically targeted SHH and EP_4 signaling components. We
364 intentionally avoided use of over-expression systems because GPCR over-expression can both
365 alter ciliary length and affect the protein composition of primary cilia (Guadiana et al., 2013). By
366 avoiding these pitfalls, we were able to uncover a direct contribution of SHH signaling to ciliary
367 length and cAMP control that may have been masked by use of over-expression systems.

368

369 Prostaglandin signaling has been appreciated as a modulator of motile and primary cilia function
370 for some time, and is documented to control motile cilia development and beat frequency in
371 multiple cell types (Gayner and McCaffrey, 1998; Haxel et al., 2001; Jin et al., 2014; Marra et
372 al., 2019). Further, clinical relevance for prostaglandin impact on primary cilium function is
373 suggested by over expression of PGE_2 pathway components in autosomal dominant polycystic
374 kidney disease, and by a growing body of work suggesting PGE_2 has therapeutic potential for
375 treatment of some ciliopathies (May-Simera et al., 2018; Song et al., 2009; Stokman et al.,
376 2021). The direct genetic link between PGE_2/EP_4 signaling and both motile and primary
377 ciliogenesis was revealed through analysis of the zebrafish *lkt* mutation, which compromises
378 ciliary growth by disrupting function of the PGE_2 transporter ABCC4 (Jin et al., 2014). *Lkt* fish
379 show reduced cilia numbers and a range of phenotypes associated with ciliary dysfunction
380 including hydrocephalus, curved bodies and abnormal left-looping hearts. Reduction of ABCC4
381 expression decreases length of primary cilia in mouse fibroblasts (Jin et al., 2014), and as we
382 show here, attenuates SHH target gene induction. Intriguingly, in addition to its positive impact

383 on ciliary cAMP through export of PGE_2, ABCC4 has also been demonstrated to deplete cAMP
384 from ciliary membrane through its multi-specificity exporter function (Wijaya et al., 2020). This
385 activity was revealed by a study focused on the SHH subtype of medulloblastoma in which
386 ABCC4 over-expression was found to reduce membrane cAMP to slow PKA-promoted
387 repressor processing of GLI2/3 transcription factors (Wijaya et al., 2020). Thus, like what we
388 show here for SHH, ABCC4 may buffer its own contributions to ciliary cAMP control by both
389 promoting and attenuating accumulation of the second messenger.

390

391 Despite a growing body of work supporting that cAMP flux occurs downstream of SHH, the
392 relationship between pathway activation and cAMP control remains complex and controversial.
393 This is due, at least in part, to the dual positive and negative regulatory contributions of PKA to
394 GLI effector activity and the ambiguous role of SMO-mediated $G\alpha_i$ activation downstream of
395 ligand (Arensdorf et al., 2016; Aza-Blanc et al., 2000; Low et al., 2008; Niewiadomski et al.,
396 2014; Ogden et al., 2008; Riobo et al., 2006). Moreover, evidence for direct SMO/$G\alpha_i$-induced
397 attenuation of PKA-directed GLI processing through cAMP reduction has been difficult to obtain.
398 Whether this is due to SMO-regulated, $G\alpha_i$-mediated cAMP control occurring in temporally and
399 spatially limited cellular contexts, or to $G\alpha_i$-independent modes of PKA regulation downstream
400 of SHH, remains unclear. In some cell types, SHH-directed removal of GPR161 from ciliary
401 membrane may lower cAMP to sufficiently halt PKA-directed GLI processing (Mukhopadhyay et
402 al., 2013). However, more recent work suggests the intracellular carboxyl tail of activated SMO
403 may act as a PKA inhibitor to block GLI phosphorylation upon pathway induction, suggesting a
404 cAMP-independent route to PKA control (Happ, 2021). Nevertheless, we and others have
405 reported cAMP reduction occurring in response to SMO activation (Barzi et al., 2011; Belgacem
406 and Borodinsky, 2015; Marada et al., 2015; Ogden et al., 2008; Riobo et al., 2006), suggesting

407 a need for cAMP buffering to prevent adverse effects on primary cilia homeostasis that might
408 occur following SHH-mediated cAMP reduction.

409

410 Consistent with the ability of SHH to transiently reduce ciliary cAMP through activation of SMO
411 and desensitization of GPR161, we did observe modest ciliary length reduction in cultured cells
412 exposed to SHH (Figures 1-4). However, these length reductions typically failed to reach
413 significance and were never as severe as what occurred following blockade of prostaglandin
414 signaling. We hypothesize this is due to buffering of cAMP flux by SHH-stimulated PGE_2/EP_4
415 signaling. It is also possible that additional $G\alpha_s$-coupled ciliary GPCRs could be engaged
416 downstream of SHH to prevent sustained cAMP reduction that could lead to ciliary dysfunction.
417 This is because multiple additional $G\alpha_s$-coupled GPCRs enrich in ciliary membrane. In addition
418 to EP_4 and GPR161, as discussed here, $G\alpha_s$-coupled, V2R, D1R, and 5-HT_6 receptors are also
419 commonly found in primary cilia in cell and tissue-specific manners (Domire et al., 2011; Jiang
420 et al., 2019; Jin et al., 2014; Mukhopadhyay et al., 2013). Intriguingly, and perhaps indicative of
421 coordination of activity occurring between ciliary GPCRs, a recent report suggests SMO
422 stimulation can amplify or sensitize responses by D1R and 5-HT_6 (Jiang et al., 2019). Whether
423 these effects result from direct communication between SMO and other GPCR classes, or from
424 ciliary GPCRs tuning their activity to ciliary cAMP status is not yet known. Importantly, cAMP
425 shifts induced by these GPCRs are confined to the primary cilium such that cytoplasmic cAMP
426 is unaltered, allowing for localized modulation of cAMP-regulated responses (Hansen et al.,
427 2020; Truong et al., 2021; Wheway et al., 2018). Future investigation focused on understanding
428 the complex regulation of ciliary cAMP control will likely provide insight into this fascinating cell
429 biology.

430

431 Remarkably, signal crosstalk occurring downstream of Hedgehog family ligands that buffers
432 cAMP flux to safeguard against pronounced changes in cAMP availability may be evolutionarily
433 conserved. In *Drosophila*, HH signaling is activated at the plasma membrane because cells of
434 most fly tissues lack functional primary cilia (Huangfu and Anderson, 2005). This mitigates the
435 need for a HH connection to pathways involved in ciliary homeostasis but does not eliminate the
436 requirement for cAMP control downstream of ligand. This is because, like what occurs in
437 vertebrate systems, PKA phosphorylation of the *Drosophila* GLI ortholog Cubitus interruptus (Ci)
438 leads to its conversion into a truncated transcriptional repressor (Aza-Blanc et al., 1997;
439 Smelkinson et al., 2007). Accordingly, genetic evidence indicates *Drosophila* SMO (dSMO)
440 activates $G\alpha_i$ to lower cAMP in response to HH, providing a mechanism by which ligand
441 stimulation may rapidly halt Ci processing (Ogden et al., 2008). However, a *Drosophila*-specific
442 positive regulatory role for PKA-mediated phosphorylation of dSMO that promotes high-level
443 pathway activity is also proposed, and is seemingly at odds with dSMO activation of $G\alpha_i$ (Jia et
444 al., 2004). A potential mechanism by which dSMO solves this problem was revealed through a
445 recent study demonstrating that, in some cell types, dSMO stimulation leads to cAMP
446 accumulation through $G\alpha_s$ activation (Praktiknjo et al., 2018). This activation is dependent upon
447 dSMO phosphorylation by G protein-coupled receptor kinase Gprk2 and is thought to enhance
448 pathway responsiveness to lower threshold HH stimulation (Praktiknjo et al., 2018). It is not yet
449 clear whether $G\alpha_s$ activation downstream of HH occurs through dSMO signal bias, or if it is
450 induced indirectly through dSMO crosstalk with $G\alpha_s$-coupled GPCR signaling partners.
451 Nevertheless, the observation that dSMO can lead to $G\alpha_s$ activation in flies supports an
452 evolutionarily conserved ability of Hedgehog family members to affect exquisite control of cAMP
453 flux to ensure appropriate downstream signaling activity.

454

455 Whereas this study is the first to reveal a mechanism by which SHH signaling actively
456 contributes to primary cilium homeostasis, SHH is not the only pathway regulated by the primary
457 cilium to tap into processes controlling ciliary growth and function. WNT signaling, which can be
458 both activated and repressed through the primary cilium, promotes primary ciliogenesis through
459 WNT3A-mediated reorganization of centriolar satellites, leading to increased ciliary length and
460 thickness (Kyun et al., 2020). Moreover, developmental signaling pathways including WNT,
461 TGFβ, and NOTCH impact growth of motile cilia through action of their downstream
462 transcriptional effectors (Jin et al., 2014; Tozser et al., 2015). The observations that multiple
463 developmental signaling pathways influence both primary and motile cilia growth suggest that
464 linking specific signal transduction cascades to ciliary regulators may be a common evolutionary
465 theme among pathways that work through or depend on ciliary function.

466

467 **Methods**

468 *Chemicals*

469 L161,982 (Tocris) and Celecoxib (Coxib, Cayman Chemical Company) were reconstituted in
470 DMSO and stored at -20°C. Cyclopamine (LC Laboratories) was reconstituted in ethanol and
471 stored at -80°C. Arachidonic acid (Cayman Chemical Company) was stored in ethanol at -20°C.
472 Prostaglandin E2 (Sigma Chemicals) and Forskolin (Sigma Chemicals) were reconstituted in
473 ethanol and stored at 4°C. Giripladib (GIRI) was synthesized and stored according to published
474 procedures (Duvernay et al., 2015; Thotala et al., 2013).

475

476 *Cell culture and DNA expression plasmids*

477 Wild type and Flp-In IMCD3 cells were cultured in Dulbecco's Modified Eagle Medium: F12
478 supplemented with 10% fetal bovine serum (FBS) and 1% Penicillin Streptomycin solution
479 (Gibco). NIH-3T3, Flp-In-3T3, RPE-1, *ABCC4*$^{-/-}$, NIH-3T3, and all MEF cell line media were
480 supplemented with 10% fetal calf serum. Cells were passaged routinely with 0.25%
481 Trypsin/EDTA solution and maintained under standard incubation conditions (5% CO2, 37°C) in
482 a humidified incubator. All cell lines were routinely tested for mycoplasma contamination. To
483 promote ciliogenesis, cell lines were serum starved for 2 hours in serum-free media (DMEM
484 supplemented with 0.1 mM nonessential amino acids, 2mM L-Glutamine, 1mM sodium pyruvate
485 and 1% Pen-Strep). After starvation, media was replaced with low serum (0.5%) media and
486 cells were incubated for 24 or 36 hours.

487

488 Cyto-bPAC (pgLAP5-EF1a dTATA-bPAC-GFP) and Cilia-bPAC (pgLAP5-EF1a dTATA-Arl13b-
489 bPAC-GFP cloned into a version of pGLAP5 with a minimal chicken lens d-crystallin promoter)
490 have been previously described (Truong et al., 2021). IMCD3 cell lines stably expressing Cyto-
491 bPAC-GFP and Cilia-bPAC-GFP were generated using the Flp-In system following
492 manufacturer's instructions (Invitrogen). IMCD3 Flp-In cells (Breslow and Nachury, 2015) were
493 transfected using Lipofectamine 3000 with the appropriate plasmids and selected with 40
494 mg/mL hygromycin (GIBCO). Single colonies were expanded, and protein expression was
495 confirmed by fluorescence microscopy for GFP.

496

497 *Immunofluorescence*

498 IMCD3, RPE1, and MEF cells were plated onto coverslips (Corning) and pretreated with either
499 vehicle or drug in serum-free media. After 2 hours, media was changed to low serum media
500 containing drug and SHH-N conditioned media (100 µL/mL), and then incubated for ~20 hours.

501 After incubation, cells were washed with PBS, and then fixed in 4% paraformaldehyde for 12
502 minutes. Cells were then washed with wash buffer (PBS with 0.1% Triton X-100) three times for
503 5 mins and incubated in blocking buffer for 60 min at room temperature (PBS with 2% BSA, 1%
504 Tween-20, 1% goat serum). Primary antibody incubations were performed overnight at 4°C. The
505 following antibodies and dilutions were used: anti-Smo (Santa Cruz, 1:500) and anti-acetylated
506 α-tubulin (Cell Signaling, 1:1000), diluted in blocking buffer. Secondary antibody incubations
507 were performed with AlexaFluor 555 and 647 (1:10000) conjugated secondary antibodies (Life
508 Technologies) and DAPI for 60 min at RT. Following antibody incubation, samples were washed
509 three times in PBS + 0.05% Tween-20 for 5 minutes. Cells were washed 3x in wash buffer then
510 3x in PBS prior to mounting with Prolong Diamond without DAPI (Life Technologies). Images
511 were collected using a Zeiss LSM 710 or Leica TCS SP8 STED 3x confocal microscope with a
512 63x oil-immersion objective and processed using ZEN 2012 (blue edition, Zeiss), LAS X (Leica),
513 and Photoshop CS6. For all immunofluorescence experiments, multiple cells (≥100) were
514 examined over at least two independent experiments. Representative images are shown.

515

516 *In vivo analysis*

517 *EP4*$^{+/-}$ and *EP4*$^{-/-}$ embryos in the C57BL/6 background were harvested and processed for
518 immunohistochemistry at E9.5. Pregnant dams were harvested, uterine horns removed, and
519 embryos were dissected in 1X PBS, then rinsed three times in 1X PBS. Embryos were fixed
520 overnight at 4°C in 4% PFA. The following day, embryos were rinsed three times in 1X PBS and
521 transferred to 30% sucrose to cryo-protect. The following day, embryos were frozen in O.C.T.
522 Compound (Tissue-Tek) on dry ice. Embryos were sectioned transverse at 10 µm thickness on
523 a Leica Microm CM1950 cryo-stat. Sections were briefly dried, then washed in 1X TBST, then
524 blocked with 2% BSA, 1% goat serum, 0.1% Triton-X-100 in 1X PBS. Antibodies were diluted in

525 blocking buffer and incubated overnight on sections at room temperature. The following
526 antibodies and dilutions were used: mouse anti-PAX6 (1:25; DSHB), and rabbit anti-OLIG2
527 (1:300; Millipore). Primary antibody was removed, sections were washed with 1X TBST three
528 times, then incubated for 3 hours in secondary antibodies (Invitrogen) at a 1:500 dilution.
529 Sections were washed three times in 1X TBST, then rinsed with water, and cover slips were
530 applied with Pro Long Gold mounting media with DAPI. Sections were imaged on a Leica DMi8
531 widefield microscope. A minimum of four embryos per genotype were analyzed.

532

533 For electron microscopy of neural tube primary cilia, samples were fixed in 2.5% glutaraldehyde,
534 2% paraformaldehyde in 0.1M cacodylate buffer containing 2 mM $MgCl_2$. Following fixation,
535 samples were dissected to expose the interior of the neural tube lumen. Dissected samples
536 were buffer washed, post-fixed in 0.1% aqueous osmium tetroxide for 1 hour, washed with
537 ddH_2O, dehydrated with an ascending ethanol series, and critical point dried in liquid CO_2 using
538 an Autosamdri 931 (Tousimis, Rockville, MD). Dried samples were sputter-coated under
539 planetary rotation with 15nm iridium and imaged in a ThermoFisher Scientific Teneo scanning
540 electron microscope at 2kV using the Everhart-Thornley and T1 detectors.

541

542 *Ciliary cAMP assay*

543 IMCD3 cells were seeded at 18,000 cells/well in an 8-well chamber slide (Nunc™ Lab-Tek™ II
544 Chamber Slide™ System) and transduced the next day with the ratio metric cilia-targeted
545 cADDis BacMam (Molecular Montana, D0211G) per manufacturer's recommendation. Cells
546 were infected with 20 µl of BacMam sensor stock in a total of 250 µl of media containing 2 mM
547 Sodium Butyrate (Molecular Montana) for 30 minutes at room temperature in dark followed by 5
548 hours at 37 C°. BacMam was removed and replaced with low serum media containing 1 mM

549 Sodium Butyrate for 16-24 hours with or without GIRI or L-161,982 treatment. Prior to imaging,
550 cells were incubated in PBS for 20 minutes at room temperature. Positive agonist FSK (100 μM)
551 was added 30 seconds after the recording was initiated and images were acquired on a Nikon
552 A1R confocal on live cell imaging mode (63x, epifluorescence) every 10 seconds for 8 minutes.
553 For experiments with SAG, the signal was recorded for basal conditions followed by incubation
554 with FSK for 1.5 minutes and then treated with either SAG or vehicle and recorded every 10
555 seconds for 8 minutes. The red fluorescence and green fluorescence intensities over time were
556 processed on the Nikon NIS-Elements imaging software by determining a mask for each cilium
557 and determining the ratio of the green fluorescence to the red fluorescence. The data were
558 normalized to the time point at the beginning of each experiment (set to 100%) and the inverse
559 of the value was used to plot the GraphPad Prism.
560

561 *Optogenetic stimulation*

562 bPAC-expressing IMCD3 Flp-In cells were plated onto coverslips, grown to confluency, and
563 pretreated with either vehicle or L161-982 (10μM) in serum-free media. After 2 hours, media
564 was changed to low serum media containing drug and SHH-N conditioned media (100 μL/mL),
565 and then incubated for ~18 hours. Prior to immunofluorescence analysis, cells were transferred
566 to a custom-made LED humidified incubator with 5% CO_2 for continuous blue light 450nm
567 stimulation at ~0.4 mW/cm^2 for 3 hours (Zhang et al., 2019). Following this,
568 immunofluorescence staining was carried out as described above.

569

570 *Quantitative Reverse Transcriptase Polymerase Chain Reaction (qRT-PCR)*

571 The total RNA was extracted from cells using the Rneasy Mini Kit (Qiagen) according to
572 manufacturer's protocol. One thousand nanograms of RNA was used to synthesize

573 complementary DNA (cDNA) using High-Capacity cDNA Reverse Transcription Kit (Applied
574 Biosystems). qRT-PCR primers are described in Table S1. qRT-PCR reactions were performed
575 on a QuantStudio 7 Flex PCR machine using PowerUp Sybr Green Master Mix (Applied
576 Biosystems). Corresponding changes in the expression levels of selected genes were
577 calculated using the ΔΔCt method relative to housekeeping genes, Ppia and Btf3 (Arensdorf et
578 al., 2017).

579

580 *Quantification of Ciliary Length and Ciliary Signal Intensity*

581 At least three randomly chosen fields of view were selected per condition per experiment, and
582 all cilia within the field were quantified using ZEN 2012/LAS X. For ciliary length measurement,
583 a maximum projection of the Z stack images was created, and the length of cilia was traced
584 from the base to the tip using the line profile tool in the LAS X software. For ciliary SMO signal
585 intensity determination, each cilium surface area was traced from the base to the tip using
586 spline profile function. Line scan intensity values along the cilium were exported and analyzed in
587 Excel.

588

589 *Statistical Methods*

590 All statistical analyses were performed using GraphPad Prism. One-way unpaired non-
591 parametric ANOVA was performed for comparison of multiple means using Mann–Whitney test.
592 Statistics for ciliary length and Smoothened ciliary quantification were calculated from three
593 independent experiments with at least 100 cilia per condition per experiment. Smoothened
594 translocation intensity was normalized to acetylated α-tubulin intensity. All quantified data are

595 presented as mean ± SEM, with $p < 0.05$ considered statistically significant. Significance
596 depicted as *$p < 0.05$, **$p < 0.01$, ***$p < 0.001$, ****$p < 0.0001$, n.s = not significant.

597

598 *Cell Line Generation*

599 EP_4 knockout cells were generated from *$EP_4^{-/-}$* embryos as previously reported (Segi et al.,
600 1998). Embryos (13.5 dpc) were freshly isolated and placed in individual 10 cm culture dishes
601 where they were eviscerated. Heads were removed and used for genotyping to identify
602 homozygous null embryos and wild type littermates using conventional PCR. Embryo bodies
603 were transferred to 15 mL conical tubes containing 5mL fresh PBS and dissociated by
604 aspirating through a 16-G needle into a 10mL syringe and expelling the contents. Warm media
605 (DMEM+10%FBS+1%pen/strep) was then added to each conical tube to bring the total volume
606 to 10 mL. This solution was transferred to a 15cm culture dish containing 25mL additional media
607 and placed in a 37°C incubator. After 24h, media and non-adherent tissue pieces were
608 removed, and fresh media was added. Cells were grown to 80-90% confluence, after which they
609 were passaged and frozen down after passage number two. *$ABCC4^{-/-}$* NIH-3T3 cells were
610 generated as previously described (Wijaya et al., 2020).

611

612 *PGE_2 ELISA*

613 IMCD3 cells were cultured in a 12-well culture plate and were pre-treated for 2 hours with either
614 Cyclopamine (10μM), Celecoxib (Coxib, 10μM) or Giripladib (GIRI, 2/4 μM) in serum free
615 medium. Following pretreatment, medium was changed to low serum containing either
616 Cyclopamine, Coxib, or GIRI in control or SHH-N conditioned media, and then incubated for 36
617 hours. PGE_2 levels were determined using by ELISA (R&D Systems) according to the

618 manufacturer's instructions. The absorbance of each well was measured at 450 nm with
619 correction at 540 nm.

620

621 *RT^2 profiler PCR array analysis*

622 Expression profiling of genes responsible for ciliary organization and maintenance was
623 performed using the RT^2 profiler PCR array PAMM-127Z (Qiagen). IMCD3 cells grown in 6-well
624 culture plates were pre-treated for 2 hours with GIRI (4μM) in serum free media. Following
625 pretreatment, media was changed to low serum containing either vehicle, GIRI, or SHH-N
626 conditioned media, and then incubated for 24 hours. Two biological replicates were prepared for
627 each condition and the isolated RNA from these replicates were pooled. cDNA was generated
628 and qRT-PCR was performed. The relative quantification changes in expression were measured
629 by obtaining the threshold cycle. Data from the array was analyzed using the GeneGlobe Data
630 Analysis Center (Qiagen).

631 **Acknowledgements**

632 We thank M. Hatley, J. Messing, and members of the Ogden lab for reagents, advice, thoughtful
633 discussion, and comments on the manuscript. We thank S. Narumiya (Kyoto University) and the
634 Center for Animal Resources and Development (Kumamoto University) for providing *Ptger4*$^{-/-}$
635 frozen sperm used to generate the *EP*$_4^{-/-}$ mouse line. J. Reiter (UCSF) provided bPAC
636 expression vectors and M. Nachury (UCSF) provided Flp-In IMCD3 cells. We thank J. Temirov
637 and the St. Jude CTIC for assistance with confocal and electron microscopy.

638

639 **Funding**

640 This work was supported by National Institute of Health grants R35GM122546 (S.K.O.) and
641 R01HD099777 (E.L.S.) and by ALSAC of St. Jude Children's Research Hospital. The CTIC is
642 supported by SJCRH and NCI P30 CA021765. The content is solely the responsibility of the
643 authors and does not necessarily represent the official views of the funding agencies.

644

645 **Reagent Requests**

646 Cell lines and novel reagents will be available upon request pursuant to SJCRH material
647 transfer agreement.

648

649 **Animal Use**

650 Data and materials generated from animals were obtained in accordance with SJCRH/IACUC
651 approved protocol 608-100616-10/19 and Vanderbilt protocol M1600016-01.

Author Contributions

Conceptualization, S.S.A. and S.K.O.; Methodology, S.S.A., M.A.A., B.M.Y., M.D.S, Y.Z., E.L.S., A. J., C. G. R. and S.K.O.; Validation, S.S.A., M.A.A., M.D.S. and Y.Z.; Analysis, S.S.A., M.A.A., M.D.S., Y.Z. and A.J.; Investigation, S.S.A, M.A.A., M.D.S. and Y.Z.; Resources, Z.R., C.G.R., N.B., J. D. S., E.L.S. and S.K.O.; Writing – Original Draft, S.S.A. and S.K.O.; Writing – Review & Editing, S.S.A., J.D.S., E.L.S and S.K.O.; Visualization, S.S.A.; Supervision, S.K.O. All authors approved the submitted manuscript.

Declaration of Interests

The authors declare no competing interests.

663 **References**

664 Anvarian, Z., Mykytyn, K., Mukhopadhyay, S., Pedersen, L.B., and Christensen, S.T. (2019).
665 Cellular signalling by primary cilia in development, organ function and disease. Nat Rev Nephrol
666 *15*, 199-219.

667 Arensdorf, A.M., Dillard, M.E., Menke, J.M., Frank, M.W., Rock, C.O., and Ogden, S.K. (2017).
668 Sonic Hedgehog Activates Phospholipase A2 to Enhance Smoothened Ciliary Translocation.
669 Cell Rep *19*, 2074-2087.

670 Arensdorf, A.M., Marada, S., and Ogden, S.K. (2016). Smoothened Regulation: A Tale of Two
671 Signals. Trends Pharmacol Sci *37*, 62-72.

672 Aza-Blanc, P., Lin, H.Y., Ruiz i Altaba, A., and Kornberg, T.B. (2000). Expression of the
673 vertebrate Gli proteins in Drosophila reveals a distribution of activator and repressor activities.
674 Development *127*, 4293-4301.

675 Aza-Blanc, P., Ramirez-Weber, F.A., Laget, M.P., Schwartz, C., and Kornberg, T.B. (1997).
676 Proteolysis that is inhibited by hedgehog targets Cubitus interruptus protein to the nucleus and
677 converts it to a repressor. Cell *89*, 1043-1053.

678 Bangs, F., and Anderson, K.V. (2017). Primary Cilia and Mammalian Hedgehog Signaling. Cold
679 Spring Harb Perspect Biol *9*.

680 Barakat, M.T., Humke, E.W., and Scott, M.P. (2010). Learning from Jekyll to control Hyde:
681 Hedgehog signaling in development and cancer. Trends Mol Med *16*, 337-348.

682 Barzi, M., Kostrz, D., Menendez, A., and Pons, S. (2011). Sonic Hedgehog-induced proliferation
683 requires specific Galpha inhibitory proteins. J Biol Chem *286*, 8067-8074.

684 Belgacem, Y.H., and Borodinsky, L.N. (2015). Inversion of Sonic hedgehog action on its
685 canonical pathway by electrical activity. Proc Natl Acad Sci U S A *112*, 4140-4145.

686 Besschetnova, T.Y., Kolpakova-Hart, E., Guan, Y., Zhou, J., Olsen, B.R., and Shah, J.V. (2010).
687 Identification of signaling pathways regulating primary cilium length and flow-mediated
688 adaptation. Curr Biol *20*, 182-187.

689 Bijlsma, M.F., Peppelenbosch, M.P., Spek, C.A., and Roelink, H. (2008). Leukotriene synthesis
690 is required for hedgehog-dependent neurite projection in neuralized embryoid bodies but not for
691 motor neuron differentiation. Stem Cells *26*, 1138-1145.
692 Breslow, D.K., and Nachury, M.V. (2015). Analysis of soluble protein entry into primary cilia
693 using semipermeabilized cells. Methods Cell Biol *127*, 203-221.
694 Caspary, T., Larkins, C.E., and Anderson, K.V. (2007). The graded response to Sonic
695 Hedgehog depends on cilia architecture. Dev Cell *12*, 767-778.
696 Cherukuri, D.P., Chen, X.B., Goulet, A.C., Young, R.N., Han, Y., Heimark, R.L., Regan, J.W.,
697 Meuillet, E., and Nelson, M.A. (2007). The EP4 receptor antagonist, L-161,982, blocks
698 prostaglandin E2-induced signal transduction and cell proliferation in HCA-7 colon cancer cells.
699 Exp Cell Res *313*, 2969-2979.
700 Domire, J.S., Green, J.A., Lee, K.G., Johnson, A.D., Askwith, C.C., and Mykytyn, K. (2011).
701 Dopamine receptor 1 localizes to neuronal cilia in a dynamic process that requires the Bardet-
702 Biedl syndrome proteins. Cell Mol Life Sci *68*, 2951-2960.
703 Duvernay, M.T., Matafonov, A., Lindsley, C.W., and Hamm, H.E. (2015). Platelet Lipidomic
704 Profiling: Novel Insight into Cytosolic Phospholipase A2alpha Activity and Its Role in Human
705 Platelet Activation. Biochemistry *54*, 5578-5588.
706 Ericson, J., Rashbass, P., Schedl, A., Brenner-Morton, S., Kawakami, A., van Heyningen, V.,
707 Jessell, T.M., and Briscoe, J. (1997). Pax6 controls progenitor cell identity and neuronal fate in
708 response to graded Shh signaling. Cell *90*, 169-180.
709 Findakly, S., Daggubati, V., Garcia, G., LaStella, S.A., Choudhury, A., Tran, C., Li, A., Tong, P.,
710 Garcia, J.Q., Puri, N.*, et al.* (2021). Sterol and oxysterol synthases near the ciliary base activate
711 the Hedgehog pathway. J Cell Biol *220*.
712 Garcia, G., 3rd, Raleigh, D.R., and Reiter, J.F. (2018). How the Ciliary Membrane Is Organized
713 Inside-Out to Communicate Outside-In. Curr Biol *28*, R421-R434.

714 Gayner, S.M., and McCaffrey, T.V. (1998). Muscarinic ciliostimulation requires endogenous
715 prostaglandin production. Am J Rhinol *12*, 203-207.
716 Guadiana, S.M., Semple-Rowland, S., Daroszewski, D., Madorsky, I., Breunig, J.J., Mykytyn, K.,
717 and Sarkisian, M.R. (2013). Arborization of dendrites by developing neocortical neurons is
718 dependent on primary cilia and type 3 adenylyl cyclase. J Neurosci *33*, 2626-2638.
719 Hansen, J.N., Kaiser, F., Klausen, C., Stuven, B., Chong, R., Bonigk, W., Mick, D.U., Moglich,
720 A., Jurisch-Yaksi, N., Schmidt, F.I*., et al.* (2020). Nanobody-directed targeting of optogenetic
721 tools to study signaling in the primary cilium. Elife *9*.
722 Happ, J.T., Arveseth, C.D., Bruystens, J., Bertinetti, J., Nelson, I.B., Oliveri, C., Hedeen, D.S.,
723 Zhu, J., Capener, J.L., Bröckel, J.W., Vu., L., King. C.C., Ruiz-Perez, V.L., Veglia, G., Herberg,
724 F.W., Taylor, S.S., Myers, B.R. (2021). A PKA Inhibitor Motif within Smoothened Controls
725 Hedgehog Signal Transduction. bioRxiv.
726 Haxel, B.R., Schafer, D., Klimek, L., and Mann, W.J. (2001). Prostaglandin E2 activates the
727 ciliary beat frequency of cultured human nasal mucosa via the second messenger cyclic
728 adenosine monophosphate. Eur Arch Otorhinolaryngol *258*, 230-235.
729 He, M., Subramanian, R., Bangs, F., Omelchenko, T., Liem, K.F., Jr., Kapoor, T.M., and
730 Anderson, K.V. (2014). The kinesin-4 protein Kif7 regulates mammalian Hedgehog signalling by
731 organizing the cilium tip compartment. Nat Cell Biol *16*, 663-672.
732 Huangfu, D., and Anderson, K.V. (2005). Cilia and Hedgehog responsiveness in the mouse.
733 Proc Natl Acad Sci U S A *102*, 11325-11330.
734 Jia, J., Tong, C., Wang, B., Luo, L., and Jiang, J. (2004). Hedgehog signalling activity of
735 Smoothened requires phosphorylation by protein kinase A and casein kinase I. Nature *432*,
736 1045-1050.
737 Jiang, J.Y., Falcone, J.L., Curci, S., and Hofer, A.M. (2019). Direct visualization of cAMP
738 signaling in primary cilia reveals up-regulation of ciliary GPCR activity following Hedgehog
739 activation. Proc Natl Acad Sci U S A *116*, 12066-12071.

740 Jin, D., Liu, P., and Zhong, T.P. (2015). Prostaglandin signaling in ciliogenesis during
741 development. Cell Cycle *14*, 1-2.
742 Jin, D., Ni, T.T., Sun, J., Wan, H., Amack, J.D., Yu, G., Fleming, J., Chiang, C., Li, W.,
743 Papierniak, A.*, et al.* (2014). Prostaglandin signalling regulates ciliogenesis by modulating
744 intraflagellar transport. Nat Cell Biol *16*, 841-851.
745 Kinnebrew, M., Iverson, E.J., Patel, B.B., Pusapati, G.V., Kong, J.H., Johnson, K.A., Luchetti,
746 G., Eckert, K.M., McDonald, J.G., Covey, D.F.*, et al.* (2019). Cholesterol accessibility at the
747 ciliary membrane controls hedgehog signaling. Elife *8*.
748 Kinnebrew, M., Luchetti, G., Sircar, R., Frigui, S., Viti, L.V., Naito, T., Beckert, F., Saheki, Y.,
749 Siebold, C., Radhakrishnan, A.*, et al.* (2021). Patched 1 reduces the accessibility of cholesterol
750 in the outer leaflet of membranes. Elife *10*.
751 Kong, J.H., Siebold, C., and Rohatgi, R. (2019). Biochemical mechanisms of vertebrate
752 hedgehog signaling. Development *146*.
753 Kyun, M.L., Kim, S.O., Lee, H.G., Hwang, J.A., Hwang, J., Soung, N.K., Cha-Molstad, H., Lee,
754 S., Kwon, Y.T., Kim, B.Y.*, et al.* (2020). Wnt3a Stimulation Promotes Primary Ciliogenesis
755 through beta-Catenin Phosphorylation-Induced Reorganization of Centriolar Satellites. Cell Rep
756 *30*, 1447-1462 e1445.
757 Larkins, C.E., Aviles, G.D., East, M.P., Kahn, R.A., and Caspary, T. (2011). Arl13b regulates
758 ciliogenesis and the dynamic localization of Shh signaling proteins. Mol Biol Cell *22*, 4694-4703.
759 Low, W.C., Wang, C., Pan, Y., Huang, X.Y., Chen, J.K., and Wang, B. (2008). The decoupling
760 of Smoothened from Galphai proteins has little effect on Gli3 protein processing and Hedgehog-
761 regulated chick neural tube patterning. Dev Biol *321*, 188-196.
762 Marada, S., Navarro, G., Truong, A., Stewart, D.P., Arensdorf, A.M., Nachtergaele, S., Angelats,
763 E., Opferman, J.T., Rohatgi, R., McCormick, P.J.*, et al.* (2015). Functional Divergence in the
764 Role of N-Linked Glycosylation in Smoothened Signaling. PLoS Genet *11*, e1005473.

765 Marra, A.N., Adeeb, B.D., Chambers, B.E., Drummond, B.E., Ulrich, M., Addiego, A., Springer,
766 M., Poureetezadi, S.J., Chambers, J.M., Ronshaugen, M.*, et al.* (2019). Prostaglandin signaling
767 regulates renal multiciliated cell specification and maturation. Proc Natl Acad Sci U S A *116*,
768 8409-8418.
769 May-Simera, H.L., Wan, Q., Jha, B.S., Hartford, J., Khristov, V., Dejene, R., Chang, J., Patnaik,
770 S., Lu, Q., Banerjee, P.*, et al.* (2018). Primary Cilium-Mediated Retinal Pigment Epithelium
771 Maturation Is Disrupted in Ciliopathy Patient Cells. Cell Rep *22*, 189-205.
772 Mukhopadhyay, S., and Rohatgi, R. (2014). G-protein-coupled receptors, Hedgehog signaling
773 and primary cilia. Semin Cell Dev Biol *33*, 63-72.
774 Mukhopadhyay, S., Wen, X., Ratti, N., Loktev, A., Rangell, L., Scales, S.J., and Jackson, P.K.
775 (2013). The ciliary G-protein-coupled receptor Gpr161 negatively regulates the Sonic hedgehog
776 pathway via cAMP signaling. Cell *152*, 210-223.
777 Niewiadomski, P., Kong, J.H., Ahrends, R., Ma, Y., Humke, E.W., Khan, S., Teruel, M.N.,
778 Novitch, B.G., and Rohatgi, R. (2014). Gli protein activity is controlled by multisite
779 phosphorylation in vertebrate Hedgehog signaling. Cell Rep *6*, 168-181.
780 Ogden, S.K., Fei, D.L., Schilling, N.S., Ahmed, Y.F., Hwa, J., and Robbins, D.J. (2008). G
781 protein Galphai functions immediately downstream of Smoothened in Hedgehog signalling.
782 Nature *456*, 967-970.
783 Patten, I., and Placzek, M. (2000). The role of Sonic hedgehog in neural tube patterning. Cell
784 Mol Life Sci *57*, 1695-1708.
785 Petrov, K., Wierbowski, B.M., and Salic, A. (2017). Sending and Receiving Hedgehog Signals.
786 Annu Rev Cell Dev Biol *33*, 145-168.
787 Praktiknjo, S.D., Saad, F., Maier, D., Ip, P., and Hipfner, D.R. (2018). Activation of Smoothened
788 in the Hedgehog pathway unexpectedly increases Galphas-dependent cAMP levels in
789 Drosophila. J Biol Chem *293*, 13496-13508.

790 Raleigh, D.R., Sever, N., Choksi, P.K., Sigg, M.A., Hines, K.M., Thompson, B.M., Elnatan, D.,
791 Jaishankar, P., Bisignano, P., Garcia-Gonzalo, F.R.*, et al.* (2018). Cilia-Associated Oxysterols
792 Activate Smoothened. Mol Cell *72*, 316-327 e315.
793 Ribes, V., and Briscoe, J. (2009). Establishing and interpreting graded Sonic Hedgehog
794 signaling during vertebrate neural tube patterning: the role of negative feedback. Cold Spring
795 Harb Perspect Biol *1*, a002014.
796 Riobo, N.A., and Manning, D.R. (2007). Pathways of signal transduction employed by vertebrate
797 Hedgehogs. Biochem J *403*, 369-379.
798 Riobo, N.A., Saucy, B., Dilizio, C., and Manning, D.R. (2006). Activation of heterotrimeric G
799 proteins by Smoothened. Proc Natl Acad Sci U S A *103*, 12607-12612.
800 Segi, E., Sugimoto, Y., Yamasaki, A., Aze, Y., Oida, H., Nishimura, T., Murata, T., Matsuoka, T.,
801 Ushikubi, F., Hirose, M.*, et al.* (1998). Patent ductus arteriosus and neonatal death in
802 prostaglandin receptor EP4-deficient mice. Biochem Biophys Res Commun *246*, 7-12.
803 Shi, X., Garcia, G., 3rd, Van De Weghe, J.C., McGorty, R., Pazour, G.J., Doherty, D., Huang,
804 B., and Reiter, J.F. (2017). Super-resolution microscopy reveals that disruption of ciliary
805 transition-zone architecture causes Joubert syndrome. Nat Cell Biol *19*, 1178-1188.
806 Smelkinson, M.G., Zhou, Q., and Kalderon, D. (2007). Regulation of Ci-SCFSlimb binding, Ci
807 proteolysis, and hedgehog pathway activity by Ci phosphorylation. Dev Cell *13*, 481-495.
808 Song, X., Di Giovanni, V., He, N., Wang, K., Ingram, A., Rosenblum, N.D., and Pei, Y. (2009).
809 Systems biology of autosomal dominant polycystic kidney disease (ADPKD): computational
810 identification of gene expression pathways and integrated regulatory networks. Hum Mol Genet
811 *18*, 2328-2343.
812 Stokman, M.F., Saunier, S., and Benmerah, A. (2021). Renal Ciliopathies: Sorting Out
813 Therapeutic Approaches for Nephronophthisis. Front Cell Dev Biol *9*, 653138.

814 Thotala, D., Craft, J.M., Ferraro, D.J., Kotipatruni, R.P., Bhave, S.R., Jaboin, J.J., and Hallahan,
815 D.E. (2013). Cytosolic phospholipaseA2 inhibition with PLA-695 radiosensitizes tumors in lung
816 cancer animal models. PLoS One *8*, e69688.
817 Tozser, J., Earwood, R., Kato, A., Brown, J., Tanaka, K., Didier, R., Megraw, T.L., Blum, M., and
818 Kato, Y. (2015). TGF-beta Signaling Regulates the Differentiation of Motile Cilia. Cell Rep *11*,
819 1000-1007.
820 Truong, M.E., Bilekova, S., Choksi, S.P., Li, W., Bugaj, L.J., Xu, K., and Reiter, J.F. (2021).
821 Vertebrate cells differentially interpret ciliary and extraciliary cAMP. Cell *184*, 2911-2926 e2918.
822 Umberger, P.A., and Ogden, S.K. (2021). SPOP and CUL3 Modulate the Sonic Hedgehog
823 Signal Response Through Controlled Degradation of GLI Family Transcription Factors. Front
824 Cell Dev Biol *9*, 710295.
825 Vuolo, L., Herrera, A., Torroba, B., Menendez, A., and Pons, S. (2015). Ciliary adenylyl cyclases
826 control the Hedgehog pathway. J Cell Sci *128*, 2928-2937.
827 Wheway, G., Nazlamova, L., and Hancock, J.T. (2018). Signaling through the Primary Cilium.
828 Front Cell Dev Biol *6*, 8.
829 Wijaya, J., Vo, B.T., Liu, J., Xu, B., Wu, G., Wang, Y., Peng, J., Zhang, J., Janke, L.J., Orr, B.A.,
830 *et al.* (2020). An ABC Transporter Drives Medulloblastoma Pathogenesis by Regulating Sonic
831 Hedgehog Signaling. Cancer Res *80*, 1524-1537.
832 Ye, F., Breslow, D.K., Koslover, E.F., Spakowitz, A.J., Nelson, W.J., and Nachury, M.V. (2013).
833 Single molecule imaging reveals a major role for diffusion in the exploration of ciliary space by
834 signaling receptors. Elife *2*, e00654.
835 Zhang, P., Fan, B., Yang, P., Temirov, J., Messing, J., Kim, H.J., and Taylor, J.P. (2019).
836 Chronic optogenetic induction of stress granules is cytotoxic and reveals the evolution of ALS-
837 FTD pathology. Elife *8*.

838

839 **Figure Legends**

840 **Figure 1: ABCC4 loss reduces primary cilium length and attenuates SHH signal**
841 **induction**. **(A)** *ABCC4*$^{-/-}$ NIH-3T3 cells have shortened primary cilia. Cells were treated with
842 control or SHH conditioned media as indicated. The ciliary axoneme is marked by acetylated α-
843 tubulin (magenta). DAPI (blue) marks nuclei. The scale bar represents 10 μm. **(B)**. Primary cilia
844 of ≥100 cells/condition were measured to determine average ciliary length. Experiments were
845 performed at least twice, and all data pooled. Statistical significance was determined using a
846 one-way ANOVA. Error bars indicate SD. **(C)**. SMO ciliary signal intensity was determined for
847 wild type and *ABCC4*$^{-/-}$ NIH-3T3 cells treated with control or SHH as in **B**. Statistical significance
848 was calculated using one-way ANOVA. Error bars indicate SD. **(D)**. Control or *ABCC4*$^{-/-}$ NIH-
849 3T3 cells were stimulated with SHH for 18 hours and induction of SHH targets *Gli1* and *Ptch1*
850 was determined by qPCR. Fold change over vehicle control conditioned media treatment was
851 calculated using the $2^{-\Delta\Delta CT}$ method. **(E)**. A model of PGE_2 signaling downstream of SHH.
852 Arachidonic acid is generated by SMO-activated $cPLA_2$ and metabolized by COX into PGE_2.
853 ABCC4 exports PGE_2 to activate EP_4 signaling to raise ciliary cAMP for anterograde IFT
854 (orange motors). **(F)**. SHH stimulates PGE_2 secretion. Measurement of PGE_2 in conditioned
855 media from control and *ABCC4*$^{-/-}$ NIH-3T3 cells was determined by ELISA. Cells were pretreated
856 with vehicle (DMSO), cyclopamine (10 μM), or COX2 inhibitor Celecoxib (Coxib,10 μM) and
857 then stimulated with control or SHH conditioned media. PGE_2 was measured in the supernatant
858 ~36 hours after treatment. The average concentration was calculated from two independent
859 experiments, each with n=3 biological replicates. Error bars indicate SEM. For all experiments *
860 indicates $p \leq 0.05$; **** indicates $p \leq 0.0001$; ns, $p > 0.05$.

861

862 **Figure 2: PGE_2 generated downstream of SHH contributes to ciliary length control. (A)**.
863 PGE_2 secretion requires SMO and $cPLA_2$ activation. PGE_2 was measured in cell culture media
864 as in **Figure 1F**. Cells were pretreated with vehicle control (DMSO), the inverse SMO agonist
865 cyclopamine (10μM) or $cPLA_2$ inhibitor GIRI (4μM), and then exposed to SHH. PGE_2 was
866 measured in the culture supernatant ~36 hours post treatment. Statistical significance was
867 calculated using one-way ANOVA. The average concentration was calculated across three
868 experiments, and the representative graph is shown. Error bars indicate SEM. **(B-D).** cPLA2
869 inhibition shortens primary cilia. **(B)**. IMCD3 cells were treated with SHH conditioned media in
870 the presence of GIRI (2 or 4 μM), or vehicle control (DMSO). Cilia were imaged by
871 immunofluorescence. The ciliary axoneme is marked by acetylated α-tubulin (magenta). DAPI
872 (blue) marks the nucleus. The scale bar represents 10 μm. **(C-D)**. Lengths of primary cilia were
873 quantified in IMCD3 **(C-C')** and RPE1 **(D)** cells, treated with SHH conditioned media in the
874 absence or presence of GIRI or Coxib (**C'**, 10μM) as indicated. Average primary cilia length
875 was determined by measuring cilia of ≥100 cells/condition across three independent
876 experiments. Significance was calculated based upon total cell number analyzed using a one-
877 way ANOVA. Error bars indicate SD. For all experiments * indicates $p \leq 0.05$; **** indicates $p \leq$
878 0.0001; ns, $p > 0.05$.

879

880 **Figure 3: EP_4 is required for primary cilium length homeostasis and maximal SHH signal**
881 **output. (A).** EP_4 inhibition shortens primary cilia in IMCD3 cells. Average primary cilia length
882 was determined in IMCD3 cells as in **Figure 2** following treatment with L161,982 (10 μM and 20
883 μM). Cells were pretreated with vehicle control (DMSO) or EP4 inhibitor L161,982, then cultured
884 in control or SHH conditioned media for ~18 hours. **(B-C).** SMO ciliary enrichment is attenuated
885 by EP_4 inhibition. SHH-stimulated SMO (**B,** red) enrichment in primary cilia was examined in
886 IMCD3 cells. Primary cilia are marked with acetylated α-tubulin (magenta). Cells were

887 pretreated with vehicle (DMSO) or GIRI 4 μM or L161,982 at 10 μM and 20 μM for 18 hours.
888 The scale bar represents 5 μm. Statistical significance was calculated using one-way ANOVA.
889 Error bars indicate SD **(C).** Average SMO ciliary signal intensity was quantified for each
890 condition. Statistical significance was calculated using one-way ANOVA. Error bars indicate SD.
891 **(D-D').** qRT-PCR analysis of *Gli1* and *Ptch1* expression in NIH-3T3 and IMCD3 cells was
892 performed. Cells were pretreated with vehicle (DMSO), GIRI (4 μM) or L161,982 (10 μM) and
893 then cultured in control or SHH conditioned media for 18 hours. Fold-change in expression was
894 determined using the $2^{-\Delta\Delta CT}$ method. **(E-G).** EP_4 loss shortens primary cilia and attenuates SMO
895 ciliary enrichment. Ciliary length and SMO (red) ciliary translocation were examined in wild type
896 and *EP4*$^{-/-}$ MEFs 18 hours post treatment with control or SHH conditioned media. Cilia are
897 marked by acetylated α-tubulin (magenta). The scale bar represents 10 μm. A representative
898 experiment is shown. **(F-G)**. Quantification of average primary cilium length **(F)** and ciliary SMO
899 signal intensity **(G)** were determined as above. For all experiments * indicates $p \leq 0.05$; ****
900 indicates $p \leq 0.0001$; ns, $p > 0.05$. Average fold change was calculated across three biological
901 replicates over two experiments. Error bars indicate SD.

902

903 **Figure 4: PGE_2/EP_4 signaling is required for ciliary cAMP control downstream of SHH. (A).**
904 A model for SHH-mediated cAMP buffering in the primary cilium. **(B-C).** IMCD3 cells
905 expressing ciliary cAMP cADDis sensors were monitored by live cell imaging after treatment
906 with the indicated compounds. Cells were pretreated overnight with either vehicle, GIRI (4 μM,
907 B), or L-161,982 (10 μM, B'-C) and were stimulated with vehicle or Forskolin (100 μM). A
908 minimum of 6 cilia were recorded for each condition per experiment. The experiment was
909 repeated three times. A representative experiment is shown. **(C)** EP_4 signaling buffers SMO-
910 induced cAMP flux. cADDis-expressing IMCD3 cells were pretreated overnight with vehicle or L-
911 161,982 (10 μM), exposed to FSK for 1.5 minutes, then stimulated with SAG or vehicle control.

912 Fluorescence ciliary intensity was recorded over 10 mins in live cell imaging mode. An average
913 of ~6 cilia were recorded for each condition and the experiment was carried out in duplicate. A
914 representative experiment is shown. Average ciliary length **(D-E)** and SMO ciliary intensity **(F)**
915 was quantified in IMCD3-bPAC cells exposed to control or SHH conditioned media in the
916 absence or presence of L161,982, as indicated in control or blue light-exposed cells.
917 Significance was determined by one-way ANOVA. For all experiments * indicates $p \leq 0.05$; ****
918 indicates $p \leq 0.0001$; ns, $p > 0.05$. Error bars indicate SD. For all ciliary length determinations,
919 50-100 cells per condition were analyzed over at least 3 independent experiments.

920

921 **Figure. 5: EP_4 is required for primary cilium length homeostasis and SHH signaling in the**
922 **developing neural tube. (A)**. Scanning electron microscopy imaging of cardiac level neural
923 tube sections shows apical plasma membranes of cells lining the neural tube lumen. Zoom
924 images of primary cilia from $EP_4^{+/-}$ and $EP_4^{-/-}$ embryos are shown. **(B)**. Average primary cilium
925 length was calculated by measuring cilia of ~30 cells each lining ventral and dorsal regions of
926 the neural tube lumen. Primary cilia of $EP_4^{-/-}$ embryos show a statistically significant length
927 reduction. Statistical significance was calculated using one-way ANOVA. Error bars indicate SD**.**
928 **(C).** $EP_4^{-/-}$ embryos show altered ventral progenitor domains. Cardiac level sections of E9.5
929 neural tubes from the indicated genotypes were immuno-stained for neural progenitor domain
930 markers *Olig2* and *Pax6*. $EP_4^{-/-}$ neural tubes show disrupted ventral progenitor specification as
931 indicated by reduced *Olig2*-labeled cellular populations. For all experiments, four embryos per
932 genotype were analyzed.

933

934 **Supplementary Figure Legends**

935 **Supplementary Figure 1: (A). cPLA2 inhibition reduces SMO ciliary entry but does not**
936 **alter GPR161 ciliary exit.** IMCD3 cells were treated with vehicle or GIRI (4 μM) in the absence
937 or presence of SHH as indicated. GPR161 is magenta, SMO is red, Arl13b (green) marks
938 primary cilia. Scale bar is 3 μm. **(B-C). Arachidonic acid and pGE_2 rescue primary cilium**
939 **length following cPLA2 inhibition.** IMCD3 cells were treated with SHH conditioned media in
940 the presence of vehicle or 4 μM GIRI in media supplemented with increasing concentrations of
941 arachidonic acid (12.5 μM or 25 μM) as indicated. Ciliary length quantification is shown in **C**. **(D-**
942 **E)**. Ciliary length reduction of IMCD3 cells following $cPLA_2$ inhibition (4 μM GIRI) is partially
943 rescued by PGE_2 media supplementation (40μM). Ciliary length quantification is shown in **E**.
944 Statistical significance was calculated using one-way ANOVA. Error bars indicate SD. For all
945 experiments * indicates $p \leq 0.05$; **** indicates $p \leq 0.0001$; ns, $p > 0.05$. For all experiments 50-
946 100 cells per condition were analyzed over at least 2 experiments. Scale bars represent 10 μm.

947 **Supplementary Figure 2: cPLA2 inhibition changes ciliary gene expression. (A).** Heat Map
948 visualization indicates fold-changes occurring in expression of 84 ciliary genes examined using
949 the RT^2 Profiler PCR Cilia Array in the presence of vehicle (DMSO), SHH, GIRI (4 μM), or GIRI
950 (4 μM)+SHH. **(B)**. A Venn diagram indicates the number of genes modulated between GIRI and
951 GIRI+SHH over vehicle treatment. Only genes having a cut-off of ± 2.5-fold are included. **(C).**
952 Differential expression changes of the 32 genes specific to the GIRI+SHH condition are shown.

953 **Supplementary Figure 3: cADDis detects changes in ciliary cAMP.** Live imaging of cADDis-
954 expressing IMCD3 cells shows fluorescent changes of a ciliary cAMP sensor and stable
955 fluorescence of the ciliary reference marker (magenta) following exposure to vehicle **(A)** or FSK
956 (100 μM**, B**). Increasing cAMP decreases red fluorescence. **(C-C').** Relative cAMP shift is
957 shown as native **(C)** or inverse **(C')** of the fluorescent intensity ratio of the cAMP sensor to

958 reference marker. Inverse ratios are shown in the main figures to more clearly illustrate
959 increased cAMP.

960 **Supplementary Figure 4: Activation of ciliary bPAC by blue light increases primary cilium**
961 **length. (A)** Schematic of optogenetic cAMP modulation. Ciliary bPAC is activated by blue light
962 to specifically increase ciliary cAMP**. (B-F).** Primary cilia were imaged by confocal microscopy
963 after treatment with the indicated compounds and then exposed to control or blue light for 180
964 minutes. Blue light-mediated cAMP accumulation promotes ciliary elongation.

965

REAGENT or RESOURCE	SOURCE	IDENTIFIER
Antibodies		
Smoothened	SCBT	sc-166685
Acetylated a-Tubulin	Cell Signaling	5335S
GPR161	Gift from Saikat Lab	N/A
Alexa-conjugated secondary antibodies	Life Technologies	Multiple
Chemicals, Peptides, and Recombinant Proteins		
Arachidonic Acid	Cayman Chemical Co.	90010-50
Giripladib	This Paper	N/A
L161,982	Tocris Chemicals	2514
Prostaglandin E2	Sigma Chemicals	P5640
Cyclopamine	LC Laboratories	C-8700
Celecoxib	Cayman Chemical Co.	10008672
Forskolin	Sigma Chemicals	F6886-10MG
Lipofectamine 3000	ThermoFisher Scientific	L3000008
PowerUp SYBR Green Master Mix	Applied Biosystems	A25742
Critical Commercial Assays		
Prostaglandin E2 Parameter Assay Kit	R&D Systems	KGE004B
BCA Protein Assay Kit	Thermo Fisher Scientific	23227
RNeasy Plus Mini Kit	Qiagen	74136
Primary Cilia RT^2 Profiler PCR	Qiagen	PAMM-127Z
High Capacity cDNA Reverse Transcription Kit	Applied Biosystems	4368813
Ratio-metric Cilia-Targeted cADDis cAMP	Molecular Montana	D0211G
Oligonucleotides		
Ptch1 Forward: TCACCTCCATCAGCAATGTC	This Paper	N/A
Ptch1 Reverse: GAATACCACCACCACAGCAG	This Paper	N/A

Gli1 Forward: CCAAGCCAACTTTATGTCAGGG	This Paper	N/A
Gli1 Reverse: AGCCCGCTTCTTTGTTAATTTGA	This Paper	N/A
Ppia Forward: AGCACTGGAGAGAAAGGATT	(Arensdorf et al., 2017)	
Ppia Reverse: ATTATGGCGTGTAAAGTCACCA	(Arensdorf et al., 2017)	
Btf3 Forward: GAACAACATCTCTGGTATTGAAGA	(Arensdorf et al., 2017)	
Btf3 Reverse: AATGGTGAAGGTGTTTGCTG	(Arensdorf et al., 2017)	
Experimental Models: Cell Lines		
IMCD3	ATCC	CRL-2123
IMCD3 Flp-In Cells	Maxence Nachury lab	
RPE1	ATCC	CRL-4000
NIH-3T3	ATCC	CRL-1658
ABCC4$^{-/-}$ NIH-3T3	John D Schuetz lab	N/A
EP4 KO Mouse Embryonic Fibroblast	This paper	N/A
Wild Type Mouse Embryonic Fibroblast	This paper	N/A
Experimental Models: Mouse Model		
EP4$^{+/-}$ Mice	Elaine L Shelton lab	
EP4$^{-/-}$ Mice	Elaine L Shelton lab	
Recombinant DNA		
pgLAP5-EF1a dTATA-bPAC-GFP	Gift from Jeremy Reiter	N/A
pgLAP5-EF1a dTATA-Arl13b-bPAC-GFP	Gift from Jeremy Reiter	N/A
Software and Algorithms		
Prism	GraphPad	v. 8.2.0
ImageJ	https://imagej.nih.gov/ij/	v. 2.0.0-rc-59/1.51n

LAS X	Leica	
NIS-Elements Viewer	https://www.microscope.healthcare.nikon.com/products/software/nis-elements/viewer	v. 4.50.00

Arensdorf, A.M., Dillard, M.E., Menke, J.M., Frank, M.W., Rock, C.O., and Ogden, S.K. (2017). Sonic Hedgehog Activates Phospholipase A2 to Enhance Smoothened Ciliary Translocation. Cell Rep *19*, 2074-2087.

Figure.1

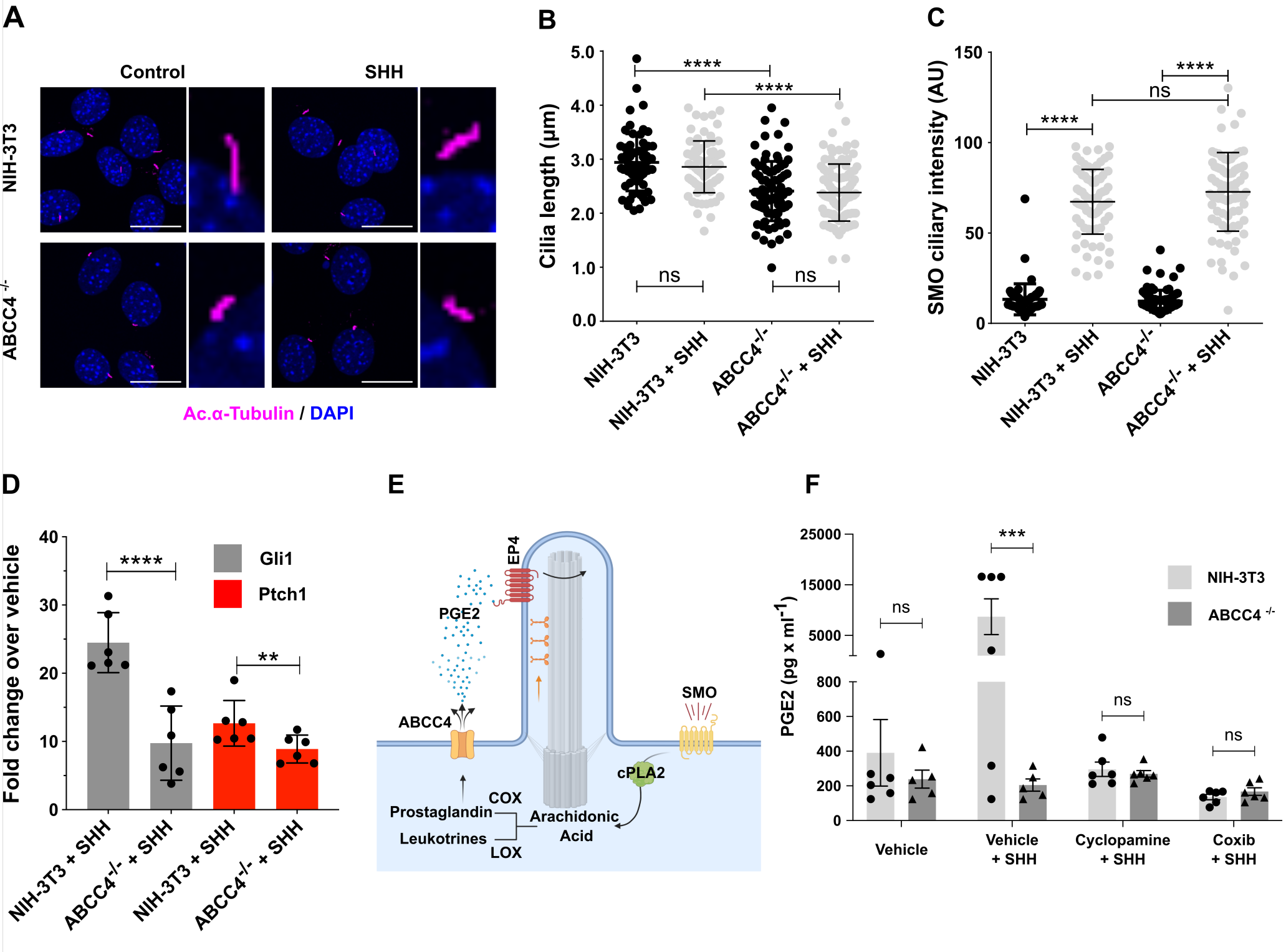
A
Control
SHH
NIH-3T3
ABCC4 -/-
Ac.α-Tubulin / DAPI
B
Cilia length (μm)
5.0
4.0
3.0
2.0
1.0
0.0
****
****
ns
ns
NIH-3T3
NIH-3T3 + SHH
ABCC4-/-
ABCC4-/- + SHH
C
SMO ciliary intensity (AU)
150
100
50
0
****
ns
****
NIH-3T3
NIH-3T3 + SHH
ABCC4-/-
ABCC4-/- + SHH
D
Fold change over vehicle
40
30
20
10
0
****
**
Gli1
Ptch1
NIH-3T3 + SHH
ABCC4-/- + SHH
NIH-3T3 + SHH
ABCC4-/- + SHH
E
EP4
PGE2
ABCC4
SMO
cPLA2
COX
Prostaglandin
Leukotrines
LOX
Arachidonic
Acid
F
PGE2 (pg x ml-1)
25000
15000
5000
800
600
400
200
0
***
ns
ns
ns
NIH-3T3
ABCC4 -/-
Vehicle
Vehicle
+ SHH
Cyclopamine
+ SHH
Coxib
+ SHH

Figure. 2

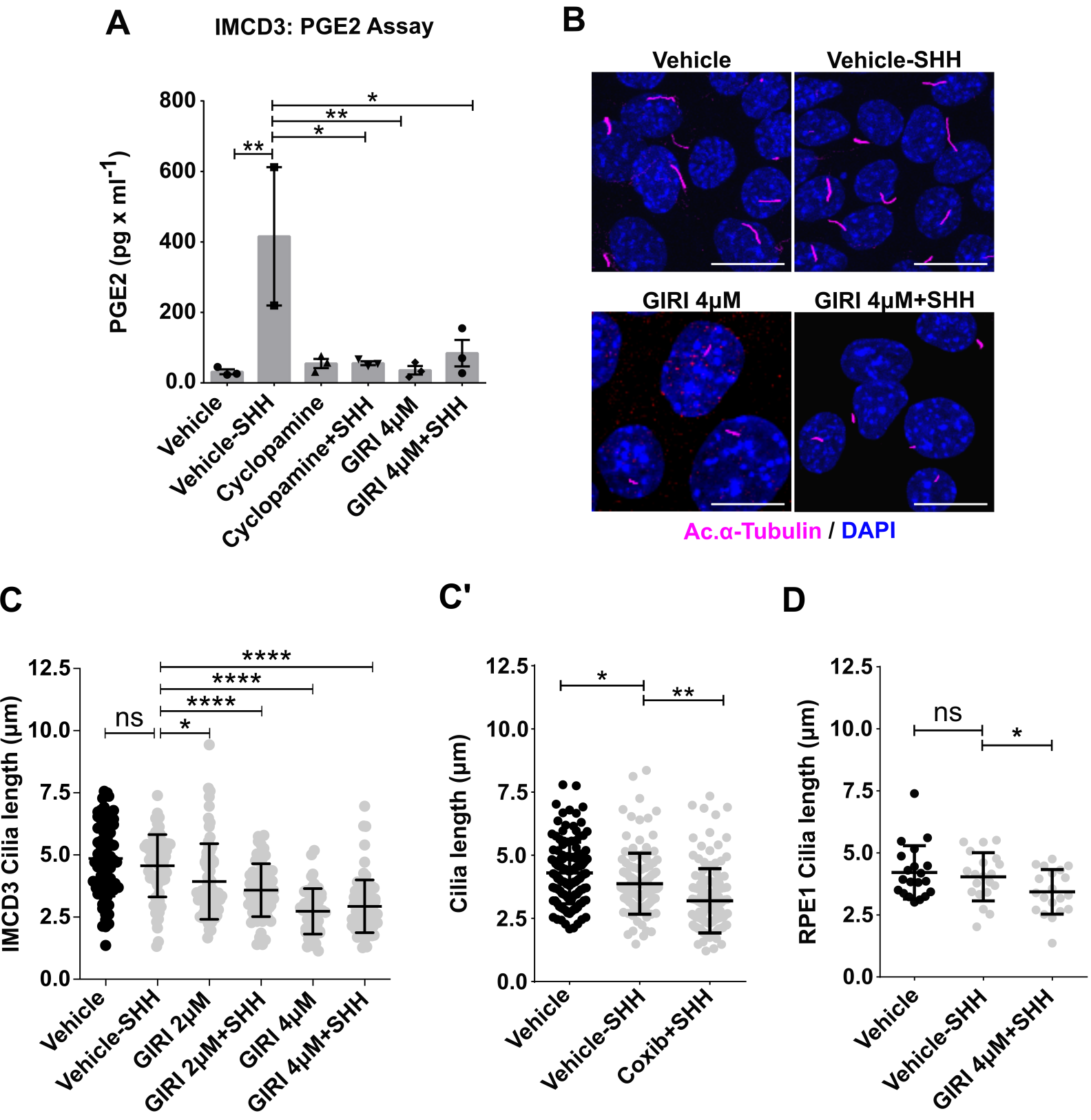
A
IMCD3: PGE2 Assay
PGE2 (pg x ml-1)
800
600
400
200
0.0
**
*
**
*
Vehicle
Vehicle-SHH
Cyclopamine
Cyclopamine+SHH
GIRI 4μM
GIRI 4μM+SHH
B
Vehicle
Vehicle-SHH
GIRI 4μM
GIRI 4μM+SHH
Ac.α-Tubulin / DAPI
C
IMCD3 Cilia length (μm)
12.5
10.0
7.5
5.0
2.5
0.0
****
****
****
ns
*
Vehicle
Vehicle-SHH
GIRI 2μM
GIRI 2μM+SHH
GIRI 4μM
GIRI 4μM+SHH
C'
Cilia length (μm)
12.5
10.0
7.5
5.0
2.5
0.0
*
**
Vehicle
Vehicle-SHH
Coxib+SHH
D
RPE1 Cilia length (μm)
12.5
10.0
7.5
5.0
2.5
0.0
ns
*
Vehicle
Vehicle-SHH
GIRI 4μM+SHH

Figure.3

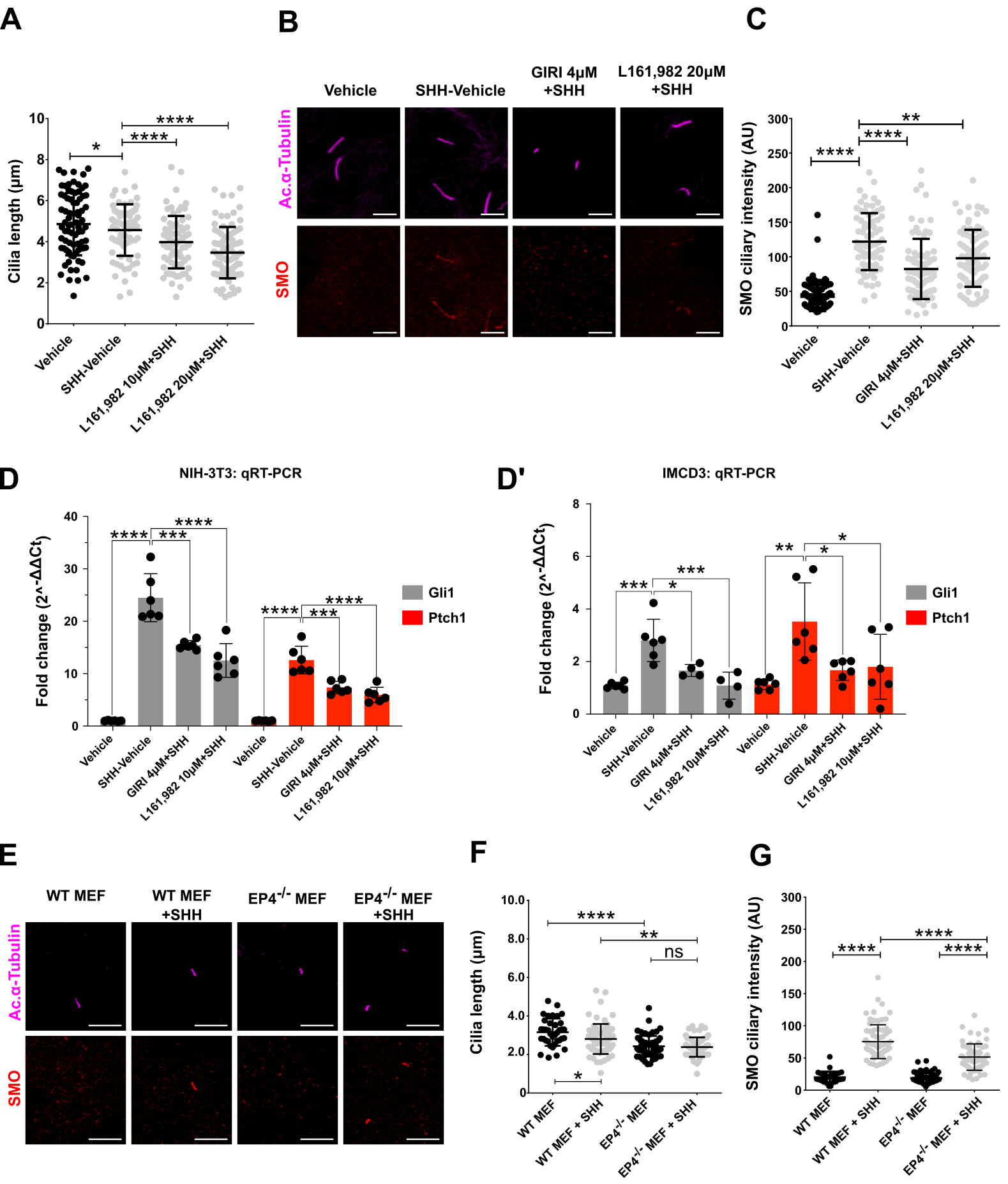
A
Cilia length (μm)
Vehicle
SHH-Vehicle
L161,982 10μM+SHH
L161,982 20μM+SHH
B
Vehicle
SHH-Vehicle
GIRI 4μM +SHH
L161,982 20μM +SHH
Ac.α-Tubulin
SMO
C
SMO ciliary intensity (AU)
D
NIH-3T3: qRT-PCR
Fold change (2^-ΔΔCt)
Gli1
Ptch1
D'
IMCD3: qRT-PCR
E
WT MEF
WT MEF +SHH
EP4-/- MEF
EP4-/- MEF +SHH
F
Cilia length (μm)
ns
WT MEF
WT MEF + SHH
EP4-/- MEF
EP4-/- MEF + SHH
G
SMO ciliary intensity (AU)

Figure.4

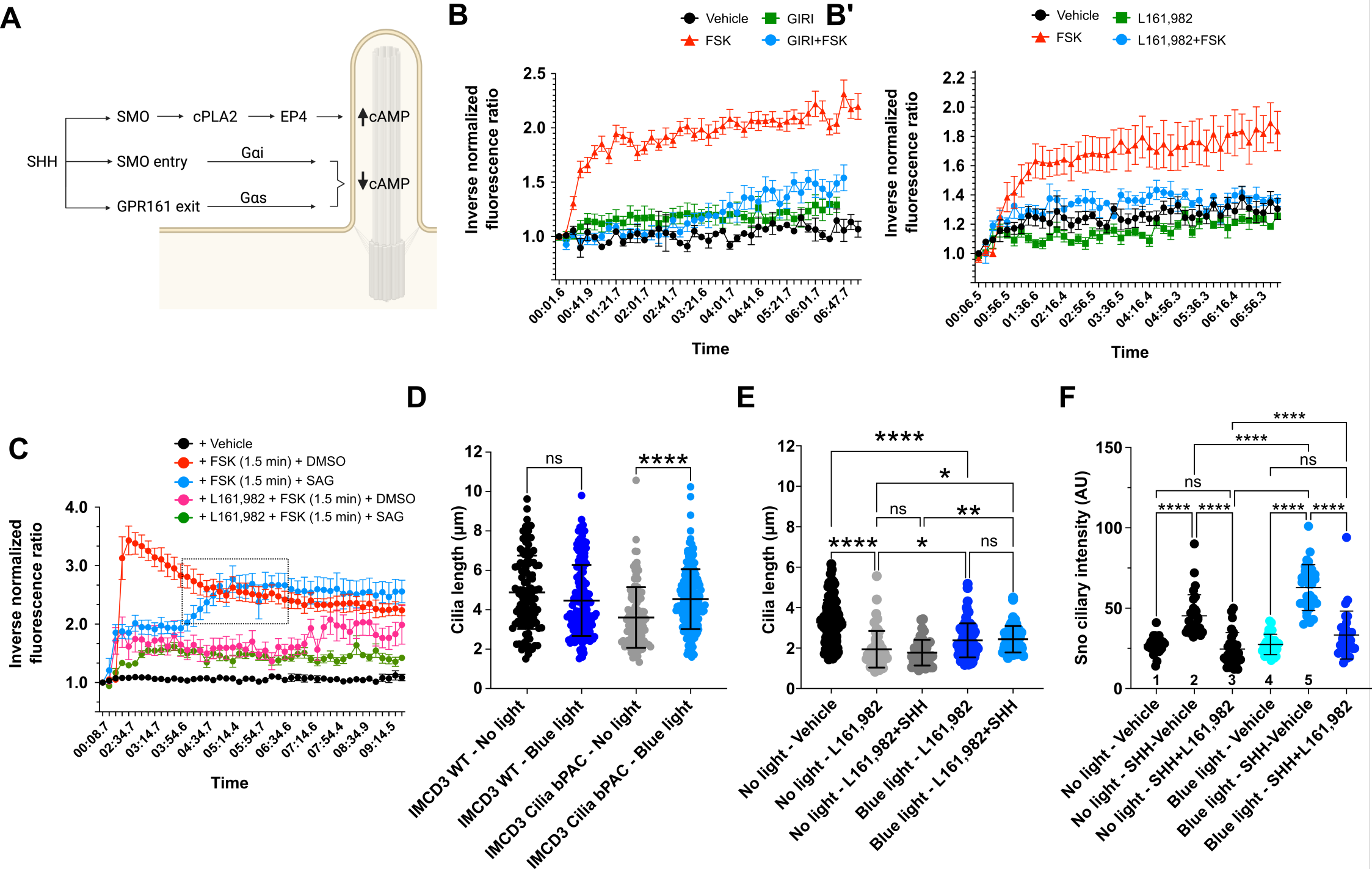
A
SHH
SMO
cPLA2
EP4
cAMP
SMO entry
Gαi
GPR161 exit
Gαs
cAMP
B
Vehicle
GIRI
FSK
GIRI+FSK
Inverse normalized fluorescence ratio
Time
B'
Vehicle
L161,982
FSK
L161,982+FSK
Inverse normalized fluorescence ratio
Time
C
+ Vehicle
+ FSK (1.5 min) + DMSO
+ FSK (1.5 min) + SAG
+ L161,982 + FSK (1.5 min) + DMSO
+ L161,982 + FSK (1.5 min) + SAG
Inverse normalized fluorescence ratio
Time
D
Cilia length (μm)
ns
****
IMCD3 WT - No light
IMCD3 WT - Blue light
IMCD3 Cilia bPAC - No light
IMCD3 Cilia bPAC - Blue light
E
Cilia length (μm)
No light - Vehicle
No light - L161,982
No light - L161,982+SHH
Blue light - L161,982
Blue light - L161,982+SHH
F
Sno ciliary intensity (AU)
No light - Vehicle
No light - SHH-Vehicle
No light - SHH+L161,982
Blue light - Vehicle
Blue light - SHH-Vehicle
Blue light - SHH+L161,982

Figure.5

A

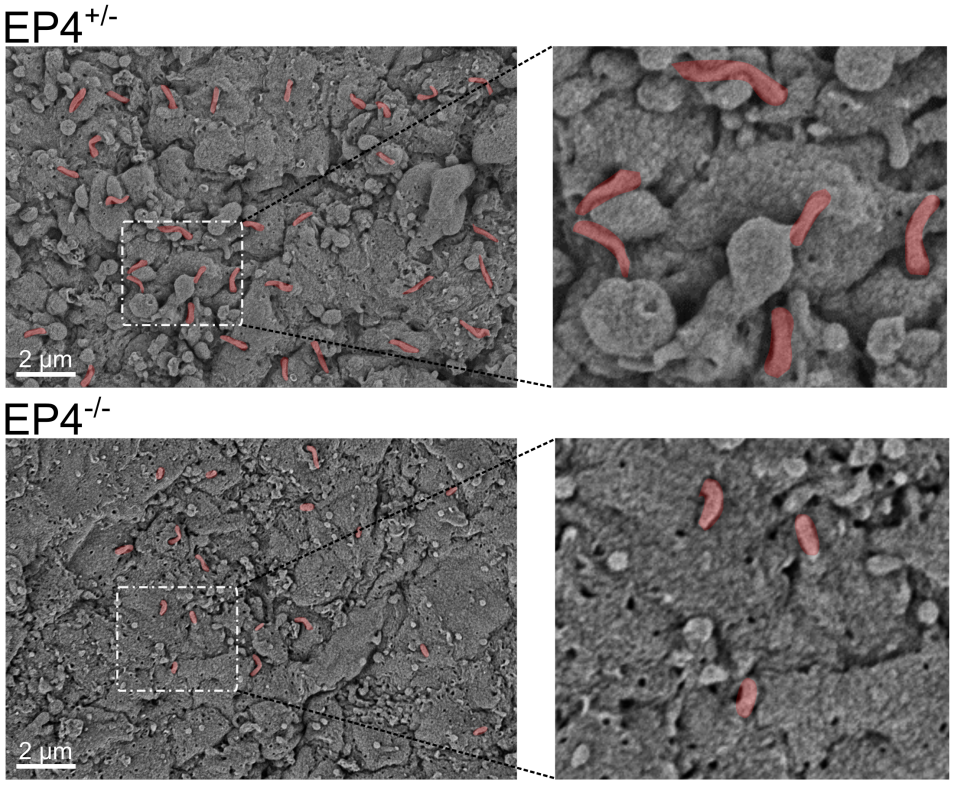
EP4+/-
2 µm
EP4-/-
2 µm

B

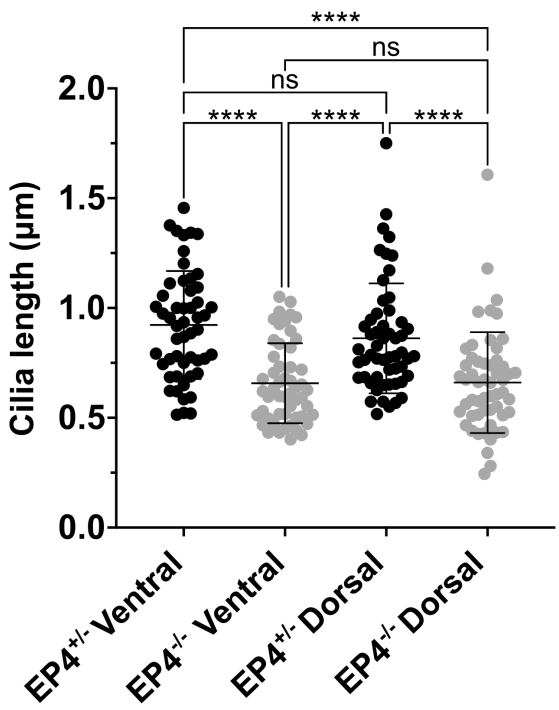
****
ns
ns
****
****
****
Cilia length (µm)
2.0
1.5
1.0
0.5
0.0
EP4+/- Ventral
EP4-/- Ventral
EP4+/- Dorsal
EP4-/- Dorsal

C

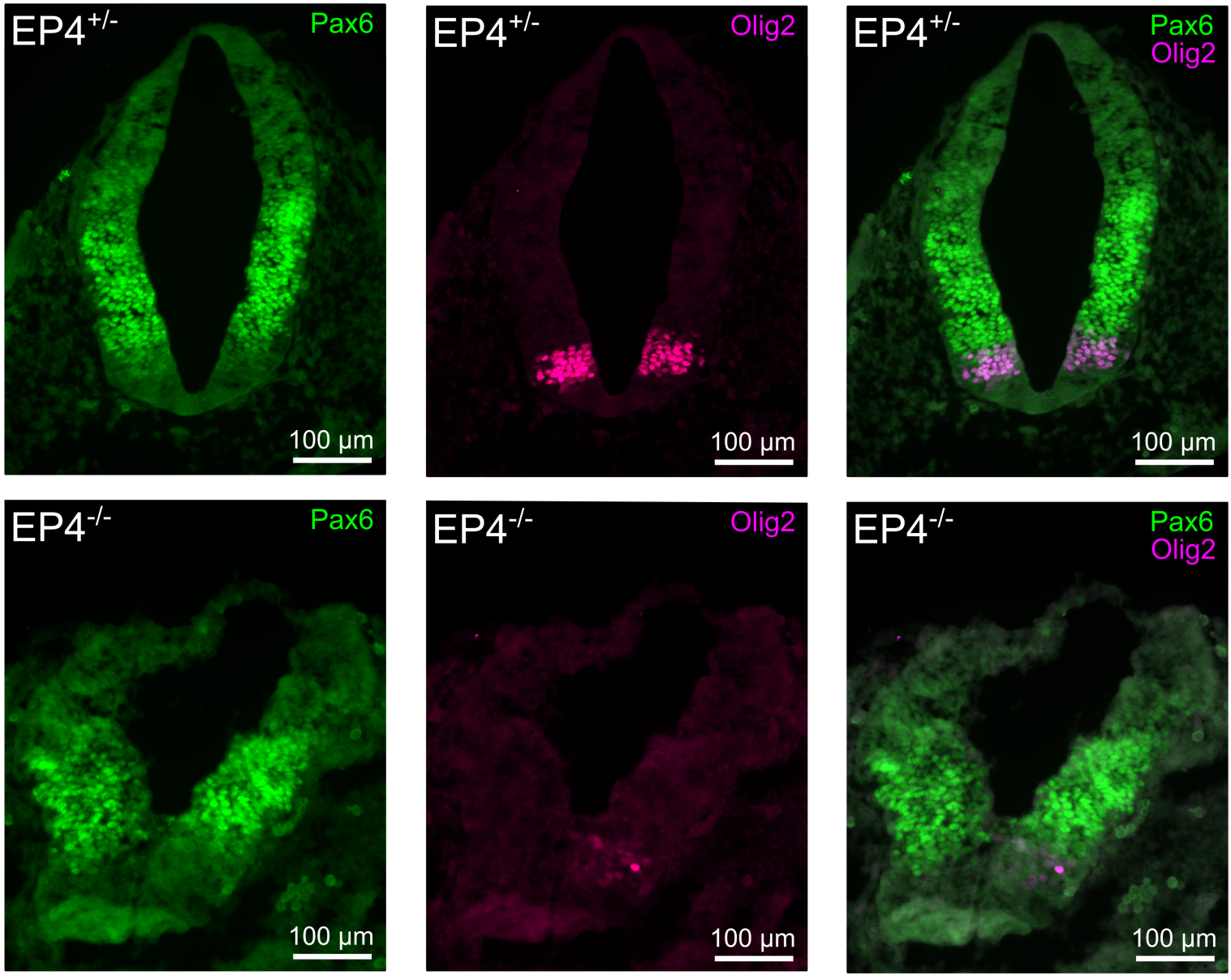
EP4+/-
Pax6
100 µm
EP4+/-
Olig2
100 µm
EP4+/-
Pax6
Olig2
100 µm
EP4-/-
Pax6
100 µm
EP4-/-
Olig2
100 µm
EP4-/-
Pax6
Olig2
100 µm